UNIVERSITY OF HEIDELBERG

Three-photon excitation of Rydberg-P-states

by

Armin Kekić

Bachelor thesis submitted in partial fulfillment for the degree of Bachelor of Science

in the
Physikalisches Institut
Department of Physics and Astronomy

under the supervision of
Dr. Adrien Signoles
and
Prof. Dr. Matthias Weidemüller

August 28, 2015

Drei-Photon-Anregung von Rydberg-P-Zuständen:

Die effektive Anregung atomarer Zustände spielt eine entscheidende Rolle in Experimenten zur Quantendynamik mittels ultrakalter Gase. Die Anregung von Rydberg-P-Zuständen durch eine Drei-Photon-Anregung ermöglicht die Realisierung eines Lasersystems, das sowohl S- als auch P-Zustände adressieren kann. Die theoretische Beschreibung eines solchen Anregungsprozesses beinhaltet viele unabhängige Parameter, was die Optimierung des Lasersystems zur Maximierung des Populationstransfers in den gewünschten Zustand erschwert. In dieser Arbeit wird die Drei-Photon-Anregung mittels analytischer Beschreibungen und numerischer Simulationen theoretisch behandelt. Eine effektive analytische Beschreibung für den Fall von großen Verstimmungen an den dazwischenliegenden Zuständen wird hergeleitet. Es wird gezeigt, dass die Anregungsdynamik in guter Näherung von nur zwei effektiven Parametern charakterisiert werden kann. Dies ermöglicht ein intuitives Verständnis der Dynamik und eine vereinfachte experimentelle Optimierung der Anregung. Die numerischen Simulationen der vollen Vier-Zustands-Beschreibung zeigt hohe Übereinstimmung mit den analytischen Vorhersagen im experimentell relevanten Parameterbereich.

Three-photon excitation of Rydberg-P-states:

The effective excitation of atomic states is a key ingredient in quantum-dynamics experiments using ultracold gases. The excitation of Rydberg-P-states using a three-photon scheme allows for implementing an experimental excitation set-up capable of addressing both S- and P-states. The theoretical description of such an excitation process involves many independent parameters, making it difficult to choose them such that the population transfer into the desired state is optimised. In this thesis the three-photon excitation is investigated theoretically by means of analytical descriptions and numerical simulations. An effective analytical description is presented for the case of three-photon resonance and large detunings on the intermediate states. It is shown that, to a good approximation, the excitation can be described using only two effective parameters, allowing for an intuitive understanding and a simplified experimental optimisation. The numerical simulations of the full system are compared to the analytical models and show good agreement in the parameter regime relevant to the experiment.

Acknowledgements

I would like to thank my fellow bachelor student **Titus Franz** for advising me with his Mathematica expertise. Thanks to **Miguel Ferreira** and **Vladislav Gavryusev** for explaining the ideas and concepts of their research projects and for helping me solve the challenges that came up during this project. Credit must also be given to Dr. **Georg Günter**, Dr. **Gerhard Zürn** and Dr. **Shannon Whittlock** for their constructive input in our group meetings. A special thanks goes to Dr. **Adrien Signoles** who has guided me through this bachelor project with his great understanding and physical intuition from which I could benefit in many fruitful discussions. Last, and by no means least, I would like to thank Prof. Dr. **Matthias Weidemüller** for many insightful discussions and for giving me the opportunity and trust to work on this bachelor project with the support of this great team.

Contents

Mome Babi

Preface

The development of laser cooling methods, such as the magneto-optical trap [1] and the dipole trap [2], have created a new research area in physics in the 1990's: ultracold atoms. Cooling atomic samples down to just above absolute zero temperature makes it possible to observe quantum mechanical behaviour on lengthscales larger than the atom size. The power of experiments with ultracold atoms lies in the high degree of control of the investigated systems: there are many techniques available, using light fields as well as static electric and magnetic fields, to control the internal and external atomic degrees of freedom. At the heart of this lies the ability to change the electronic states in the atom by applying laser- and microwave-fields; this is the main topic of this thesis.

Ultracold atomic systems have been used, both from a theoretical and experimental point of view, to tackle many different problems. By arranging ultracold atoms in regular optical lattices, it is possible to imitate the lattice structures of metallic materials and to simulate and test models from solid state theory [3]. The control over internal degrees of freedom allows for applications in quantum information, where ultracold atoms can be used to implement the basic constituent of quantum computing: the quantum bit [4, 5]. Other applications involve: the investigation of interactions and energy transport in many-body systems [6], few-body systems [7] and quantum optics [8].

The advantage of using highly excited Rydberg atoms over ground-state atoms lies in their long-range interaction properties. Whereas in conventional cold atomic systems the interactions between atoms is often negligibly small; the lengthscale of interactions between Rydberg atoms can exceed typical interatomic distances by orders of magnitude [9]. This can be used to study strongly interacting many-body systems for a lot of different interaction parameters.

The experimental basis for investigating Rydberg atoms is the excitation process, which changes the state of a fraction of the ultracold atoms from the ground- to a Rydberg-state. In this thesis a three-photon excitation scheme of Rydberg states in ^{87}Rb is discussed. In chapter 1 the system under consideration is illustrated and the theoretical prerequisites for describing such a system are outlined. In chapter 2 simplified analytical models of

the three-photon excitation in terms of two-level formulations are presented, enabling an intuitive understanding of the excitation dynamics. A full numerical simulation is used in chapter 3 to examine the validity of the simplified models and to optimise the excitation scheme used in the experimental set-up. An outlook on plans for future development of the experimental research is given in chapter 4.

Chapter 1

Introduction

1.1 Rydberg atoms

Atoms with at least one highly excited electron with a principal quantum number $n \gtrsim 10$ are called *Rydberg atoms* [9, 10]. Here, as well as in most experiments related to Rydberg atoms, alkali atoms are considered. Because of their single valence electron alkali atoms have a hydrogen-like energy level structure, which is well-understood and suited for laser cooling as there are well-separated transitions that can be used to implement magneto-optical traps. The hydrogen energy level structure in the Bohr model [11] is given by the series

$$E_n = -hc\frac{R_\infty}{n^2} \tag{1.1}$$

with Planck's constant h, the speed of light c, the principal quantum number n and the Rydberg constant

$$R_\infty = \frac{m_e e^4}{8\,c\,\varepsilon_0^2\,h^3} \tag{1.2}$$

where m_e and e are the mass and the elementary charge of the electron, and ε_0 is the vacuum permittivity. For increasing principal quantum numbers the average distance from the nucleus for the valence electron $\langle r \rangle$ also increases, scaling with $a_0(n^*)^2$ [12, 13], where a_0 is the Bohr radius. Far away from the nucleus the valence electron experiences a Coulomb $1/r$ potential, allowing to describe the atom with a hydrogen model. The deviation from the hydrogen model arises from the interaction with electrons in the lowest states, which are close to the nucleus. This deviation can be accounted for by a

Property	Expression	Scaling
Binding energy	E_{n^*}	$(n^*)^{-2}$
Level spacing	$E_{n^*} - E_{n^*+1}$	$(n^*)^{-3}$
Orbit radius	$\langle r \rangle$	$(n^*)^{2}$
Polarisability	α	$(n^*)^{7}$
Lifetime	τ	$(n^*)^{3}$
Transition dipole moment	$\lvert \langle e\lvert\hat{\mathrm{d}}\rvert n\mathrm{S}\rangle \rvert$	$(n^*)^{-1.5}$
Transition dipole moment	$\lvert \langle n\mathrm{P}\lvert\hat{\mathrm{d}}\rvert (n+1)\mathrm{S}\rangle \rvert$	$(n^*)^{-2}$
van der Waals coefficient	C_6	$(n^*)^{11}$

Table 1.1: Enhanced Rydberg-atom properties and their scaling with the effective quantum number n^* [9].

phenomenological correction term in the *effective principal quantum number* [9]

$$n^* = n - \delta(n, j, l) \tag{1.3}$$

with the *quantum defect* $\delta(n, j, l)$ that depends on the principal quantum number, the angular momentum quantum number l and the total angular momentum quantum number j including the spin-orbit interaction. The quantum defect strongly depends on angular momentum and can be assumed to vanish for $l > 3$, since for high angular momenta of the valence electron the probability of being close to the nucleus becomes small [9]. The energy level structure for ^{87}Rb then takes the same form as in the hydrogen case

$$E_{n,j,l} = -hc\frac{R_{\mathrm{Rb}}}{(n - \delta(n, j, l))^2} = -hc\frac{R_{\mathrm{Rb}}}{(n^*)^2} \tag{1.4}$$

with a modified Rydberg constant $R_{\mathrm{Rb}} = {}^{R_\infty}/_{(1+{}^{m_e}/_{m_{\mathrm{nucleus}}})}$ which is the standard Rydberg constant corrected for the effective mass of the valence electron and the Rubidium nucleus.

A consequence of the valence electron being in a Rydberg state is that, since the electron is, on average, further away from the nucleus, the size of the atom is increased up to 1000's of Bohr radii, which in dense cold atomic samples can even exceed the average interatomic distance. Furthermore, as the Coulomb potential exerts a smaller force on the valence electron, the further it is away from the nucleus the weaker the electron is bound and the polarisability is increased.

One of the most important properties of Rydberg atoms are the strong long-range interactions between them. The interaction is represented by the dipole-dipole operator [14]

$$\hat{\mathrm{V}}_{\mathrm{dd}} = \frac{\hat{\vec{\mathrm{d}}}_1 \cdot \hat{\vec{\mathrm{d}}}_2}{R^3} - \frac{3\left(\hat{\vec{\mathrm{d}}}_1 \cdot \vec{R}\right)\left(\hat{\vec{\mathrm{d}}}_2 \cdot \vec{R}\right)}{R^5} \tag{1.5}$$

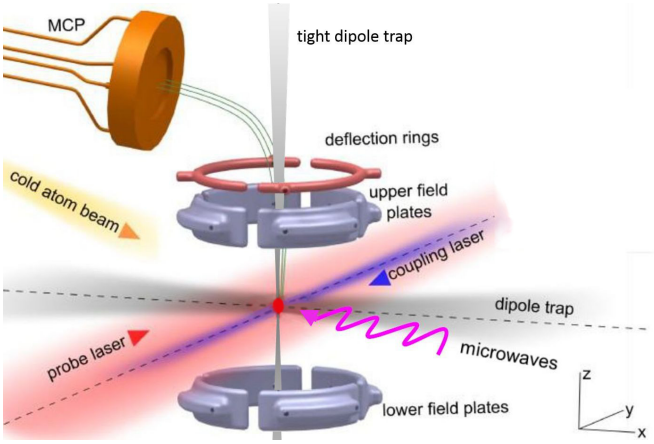

Figure 1.1: The experimental set-up: the cloud of ultracold atoms (red dot) is trapped in a vacuum chamber by a dipole trap. The field plates apply a static electric fields which can be used to ionise the Rydberg atoms. The multi-channel plate (MCP) can detect the ions. The microwave field, the probe- and coupling-lasers are used for excitation of Rydberg states.

where $\hat{\vec{d}}_{1,2}$ are the dipole operators acting on two interacting atoms 1 and 2 respectively, and $\vec{R}$ is the vector separating them. The large transition dipole moments between Rydberg states lead to these strong interactions, which form the cornerstone of experiments with ultracold Rydberg gases. In experiments with ultracold atoms in states with low principal quantum number, even the interactions between neighbouring atoms is typically negligibly small. In Rydberg gases, however, the long-range interactions dominate the behaviour of the system. Furthermore, the interaction strength and character can be tuned by changing the interacting states or applying external fields [9], such that Rydberg gases are particularly suited to study strongly interacting quantum systems.

1.2 The system

The experiment of interest is an ultracold atom experiment using ^{87}Rb-atoms in Rydberg states to study many-body phenomena in strongly interacting quantum systems [15]. The experimental set-up is schematically illustrated in figure 1.1. The goal of the experiment is to model spin systems by using Rydberg-S- and -P-states as up- and down-spins and to study their interactions. In order to study interesting phenomena involving atoms in Rydberg states, these states have to be excited first.

To excite an atom from a ground-S-state to a Rydberg-P-state the dipole selection rules for atomic transitions allow for either a one- or a three-photon excitation. The advantage of using a three-photon excitation lies in the flexibility of the laser system to address both Rydberg-S- and -P-states. While a one-photon excitation from one S-state to another is dipole forbidden, the three-photon excitation apparatus can be used to excite S-states

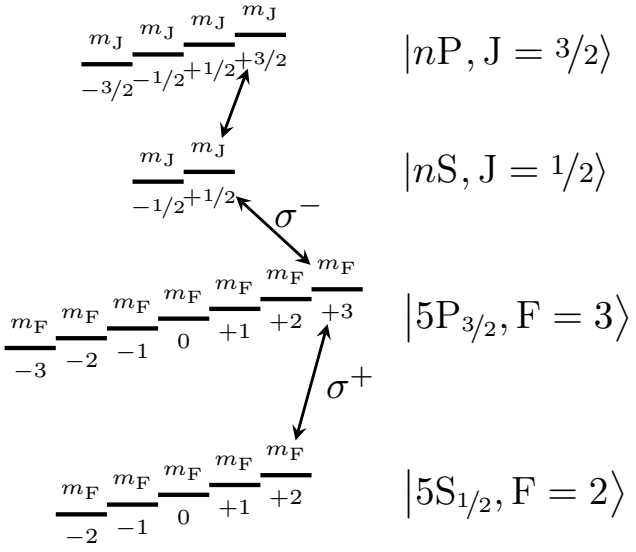

Figure 1.2: Schematic structure for the ^{87}Rb-atom levels coupled to the applied laser fields. The states are split by an external magnetic field via the Zeeman effect into fine- or hyperfine-states respectively. For the two lower state manifolds the hyperfine structure can be resolved, whereas for the highly excited states the hyperfine states are nearly degenerate and only the fine structure states are separated.

by simply tuning the two lower laser couplings on resonance with this transition while turning the third coupling off. Therefore, a three-photon laser system is the best suited apparatus to prepare such a spin model system for investigation.

The state structure that is considered here is shown in figure 1.2. The atomic states are coupled by lasers with a very narrow bandwidth. This set of states was chosen because the intermediate state manifolds are well-separated from other, unwanted, state manifolds, such that the laser couplings may be tuned off resonance with respect to the state transitions without hitting other resonances. The atomic cloud is initially prepared in the *ground state* $\left|5S_{1/2}, F = 2, m_F = +2\right\rangle$ and coupled to the *excited state* $\left|5P_{3/2}, F = 3\right\rangle$. By applying a static magnetic field, the different hyperfine states are separated in energy by the Zeeman effect and hence are no longer degenerate. σ^+-polarised light is used to address only one particular hyperfine state in the $5P_{3/2}$-manifold: because the atoms are initially prepared in the $m_F = +2$ ground state the laser can only couple this state to the $m_F = +3$ excited state. The system of these two hyperfine states is coupled to two other states with a high principal quantum number $n \approx 30$ to 100. For such states the Zeeman splitting of the hyperfine states is small compared to their linewidth; therefore the total electronic angular momentum quantum number J is a good quantum number to characterise these states. The $\left|5P_{3/2}, F = 3, m_F = 3\right\rangle$ state can only be coupled to the state with $m_J = +1/2$ in the $|nS, J = 1/2\rangle$ manifold. In order to maximise coupling efficiency, the laser coupling is σ^--polarised. The frequency of the last coupling is in the microwave regime, and, unfortunately, the polarisation of this radiation is not controlled

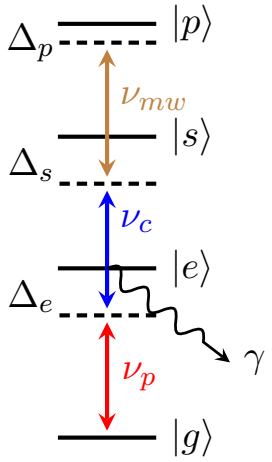

Figure 1.3: Simplified four-level system neglecting all unpopulated and uncoupled states leaving only $|g\rangle = |5S_{1/2}, F = 2, m_F = +2\rangle$, $|e\rangle = |5P_{3/2}, F = 3, m_F = +3\rangle$, $|s\rangle = |nS, J = 1/2, m_J = +1/2\rangle$ and $|p\rangle = |nP, J = 3/2, m_J = +3/2\rangle$. The states are coupled by light fields with frequencies ν_p, ν_c, ν_{mw} for the probe-, coupling- and microwave-field[1]. The state energies are $E_c = \hbar\omega_c$, $E_s = \hbar\omega_s$, $E_p = \hbar\omega_p$, with the ground-state energy set to zero for convenience. The respective n-photon detunings are $\Delta_e = \nu_p - \omega_e$, $\Delta_s = (\nu_p + \nu_c) - \omega_s$ and $\Delta_p = (\nu_p + \nu_c + \nu_{mw}) - \omega_p$. The excited state has a short lifetime compared to the other states, which can be assumed to be metastable, and spontaneously decays with a rate γ.

in the used experimental set-up. However, different fine structure states can nevertheless be addressed individually through their energy splitting by tuning the microwave coupling on resonance to one particular transition.

To describe the excitation dynamics for such a system, in principle the time evolution of all states in the four manifolds would have to be included in the calculation. By introducing Zeeman splittings and coupling only to a single state from each manifold, the system can be considerably simplified by neglecting all unpopulated and uncoupled states, allowing to reduce the problem to a four-level ladder-type system, as depicted in figure 1.3.

The decay rates of the reduced four-level system are shown in table 1.2. While the ground state can be assumed to be stable, the excited state is decaying very rapidly compared to the highly excited states. Therefore, for most purposes, the highly excited states $|s\rangle$ and $|p\rangle$ can be assumed to be metastable on the experimental timescale.

In order to excite the P-state in a controlled way, it is desirable to have an excitation process by which only the P-state is addressed while the population transfer from the ground- to the intermediate-states $|e\rangle$ and $|s\rangle$ is kept minimal. This can be achieved by tuning the three-photon system off resonance with respect to the levels that should not

[1]Throughout this thesis the Greek letters ν and ω are both used to denote the radial frequency (i.e. including 2π) of light fields, which might differ from the convention in other texts.

state	lifetime (µs)	decay rate (MHz)
$\|g\rangle$	∞	0
$\|e\rangle$	0.165	6.067
$\|s\rangle$	> 30	< 0.03
$\|p\rangle$	> 30	< 0.03

Table 1.2: Decay properties of the reduced four-level system. The exact values for the lifetime/decay rate for $|s\rangle$ and $|p\rangle$ depend on the chosen principal quantum number.

be populated and resonant to the $|g\rangle \leftrightarrow |p\rangle$ transition, *i.e.* $|\Delta_e|, |\Delta_s| \gg |\Delta_p|$. Thereby population transfer to the intermediate states can be suppressed, and the main process occurring is the excitation from the ground- to the P-state.

The goal of this thesis is to investigate and understand this system in order to optimise population transfer to the P-state. In this chapter, the basic principles needed for describing such a four-level system interacting with applied laser fields are presented.

1.3 Atoms in external radiation fields

At the heart of the excitation process lies the interaction between the atom and the applied lasers fields. In this section the simplified case of a single two-level atom in an external laser light field, which is otherwise isolated from its environment, is discussed; this can later be generalised to the case of several states and couplings. The treatment of atom-light interactions presented in this section is based on chapter 5 of D. Steck's *Quantum and Atom Optics* [16]. The two atomic states in this simplified picture are called the ground state $|g\rangle$ and excited state $|e\rangle$, with an energy difference $E = E_e - E_g = \hbar\omega_e - \hbar\omega_g = \hbar\omega$, as shown in figure 1.6. A laser light field with a frequency ω_L close to the atomic resonance is applied. A strong coherent light field with a small bandwidth

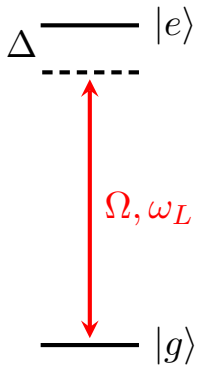

Figure 1.4: Level structure for a two-level atom with a ground- and an excited-state with an energy difference $E = \hbar\omega$ interacting with a light field of frequency ω_L and detuning $\Delta = \omega_\mathrm{L} - \omega$. Ω is the Rabi frequency of the laser coupling.

produced by a laser can be treated as a classical monochromatic electromagnetic field:

$$\vec{E}\left(\vec{r},t\right)=\vec{\mathcal{E}}\left(\vec{r},t\right)e^{-i(\omega_{\mathrm{L}}t-\vec{k}\vec{r})}+\vec{\mathcal{E}}\left(\vec{r},t\right)^{*}e^{i(\omega_{\mathrm{L}}t-\vec{k}\vec{r})} \tag{1.6}$$

where $\vec{k}$ is the light wavevector and $\vec{\mathcal{E}}\left(\vec{r},t\right)$ the in time and space slowly varying envelope function, which can be set constant for most purposes.

The Hamiltonian for the atom-light interaction in the dipole approximation can be written as [17]:

$$\hat{\mathrm{H}}_{\mathrm{AL}}=-\hat{\vec{\mathrm{d}}}\cdot\vec{E}=-\hat{\mathrm{d}}\cdot E \tag{1.7}$$

where $\hat{\vec{\mathrm{d}}}=e\hat{\vec{\mathrm{r}}}$ is the atomic dipole operator and $\hat{\mathrm{d}}=\hat{\vec{\mathrm{d}}}\cdot\vec{\epsilon}$ is its projection onto the polarisation direction $\vec{\epsilon}$ of the electric field with $\vec{\mathcal{E}}\left(\vec{r},t\right)=\mathcal{E}\left(\vec{r},t\right)\vec{\epsilon}$. It can be written as:

$$\hat{\mathrm{d}}=\sum_{n,m}\left|n\right\rangle\underbrace{\left\langle n\right|\hat{\mathrm{d}}\left|m\right\rangle}_{\mu_{n,m}}\left\langle m\right|=\sum_{n,m}\mu_{n,m}\left|n\right\rangle\left\langle m\right| \tag{1.8}$$

with $\mu_{n,m}$ being the dipole matrix element between states $\left|n\right\rangle$ and $\left|m\right\rangle$. Since $\hat{\mathrm{d}}$ is Hermitian, the dipole matrix elements obey $\mu_{m,n}=\mu_{n,m}{}^{*}$. In the case of the two-level atom the dipole operator reads:

$$\hat{\mathrm{d}}=\mu_{ge}\left|g\right\rangle\left\langle e\right|+\mu_{eg}\left|e\right\rangle\left\langle g\right|. \tag{1.9}$$

Setting the ground-state energy to zero, *i.e.* $\omega_g=0$, the free atomic Hamiltonian is $\hat{\mathrm{H}}_{\mathrm{A}}=\hbar\omega\left|e\right\rangle\left\langle e\right|$ and the total Hamiltonian

$$\hat{\mathrm{H}}=\hat{\mathrm{H}}_{\mathrm{A}}+\hat{\mathrm{H}}_{\mathrm{AL}}=\hbar\omega\left|e\right\rangle\left\langle e\right|-\left(\mu_{ge}\left|g\right\rangle\left\langle e\right|+\mu_{eg}\left|e\right\rangle\left\langle g\right|\right)\cdot\left(\mathcal{E}e^{-i\omega_{\mathrm{L}}t}+\mathcal{E}^{*}e^{i\omega_{\mathrm{L}}t}\right). \tag{1.10}$$

Here the spatial dependence of the electric field was neglected, as for optical and microwave transitions the wavelength of the light, $\lambda>400\,\mathrm{nm}$, is much larger than the size of the atom which is of the order of $1\,\text{Å}=10\,\mathrm{nm}$. This means that for the atom the light field essentially looks like a spatially constant field oscillating in time.

Rotating wave approximation (RWA): The system (1.10) can be transformed using a unitary transformation as long as it obeys the same equation of motion, *i.e.* the Schrödinger equation

$$i\hbar\frac{\mathrm{d}}{\mathrm{d}t}\left|\psi\right\rangle=\hat{\mathrm{H}}\left|\psi\right\rangle. \tag{1.11}$$

Let $\hat{\mathrm{U}}(t)$ be the time-dependent unitary transformation operator, such that the state vector transforms according to $|\psi\rangle = \hat{\mathrm{U}}(t)|\tilde{\psi}\rangle$. In order for $|\tilde{\psi}\rangle$ to obey an equation of motion of the form (1.11), the Hamiltonian operator needs to be transformed as

$$\hat{\mathrm{H}} \longrightarrow \tilde{\mathrm{H}} = \hat{\mathrm{U}}^{\dagger}\hat{\mathrm{H}}\hat{\mathrm{U}} - i\hbar\,\hat{\mathrm{U}}^{\dagger}\left(\frac{\mathrm{d}}{\mathrm{d}t}\hat{\mathrm{U}}\right). \tag{1.12}$$

The system can be transformed in the, so called, *rotating frame* by a unitary transformation represented by the operator

$$\hat{\mathrm{U}}(t) = \exp\left(-i\omega_{\mathrm{L}}t\,|e\rangle\langle e|\right) \tag{1.13}$$

For the transformation of the Hamiltonian (1.10) one finds

$$\begin{aligned}\tilde{\mathrm{H}} = &-\hbar\Delta\,|e\rangle\langle e| - \left(\overbrace{\mu_{ge}\mathcal{E}^{*}\,|g\rangle\langle e|}^{1.} + \overbrace{\mu_{eg}\mathcal{E}\,|e\rangle\langle g|}^{2.}\right)\\ &- \left(\underbrace{\mu_{ge}\mathcal{E}e^{-2i\omega_{\mathrm{L}}t}\,|g\rangle\langle e|}_{3.} + \underbrace{\mu_{eg}\mathcal{E}^{*}e^{2i\omega_{\mathrm{L}}t}\,|e\rangle\langle g|}_{4.}\right)\end{aligned} \tag{1.14}$$

where the detuning is defined as $\Delta := \omega_{\mathrm{L}} - \omega$. It indicates how far off resonance the laser frequency is. The last two terms in equation (1.14) are called *antiresonant terms* and are very rapidly oscillating at frequency $2\omega_{\mathrm{L}}$. Hence, their effect averages to zero on timescales larger than $1/2\omega_{\mathrm{L}}$. Since atomic transitions happen on much larger timescales these terms can safely be neglected. Treating also the light field quantum mechanically one can show that the four terms in the atom-light Hamiltonian correspond to four different processes [18]:

1. $|e\rangle \longrightarrow |g\rangle$ while emitting a photon
2. $|g\rangle \longrightarrow |e\rangle$ while absorbing a photon
3. $|e\rangle \longrightarrow |g\rangle$ while absorbing a photon
4. $|g\rangle \longrightarrow |e\rangle$ while emitting a photon.

This makes clear that the first two terms are the dominant processes near resonance. The total Hamiltonian in the rotating frame and RWA reads

$$\tilde{\mathrm{H}}_{\mathrm{RWA}} = -\hbar\Delta\,|e\rangle\langle e| - \hbar\left(\Omega^{*}\,|g\rangle\langle e| + \Omega\,|e\rangle\langle g|\right) \tag{1.15}$$

with the *Rabi frequency* $\Omega := \mathcal{E}\mu_{eg}/\hbar$. The Rabi frequency is a measure of how strong the laser field and the atom interact. It depends both on the dipole matrix element, which

is a property of the atomic transition, as well as on the field strength of the laser.

From now on the system is described in the rotating frame and RWA dropping the tildes and RWA-subscripts.

For a state $|\psi(t)\rangle = c_g(t)\,|g\rangle + c_e(t)\,|e\rangle$ the differential equations for the ground- and excited-state coefficients can easily be found by applying the Schrödinger equation:

$$\dot{c}_g = \langle g \,|\, \partial_t \,|\, \psi\rangle = \left\langle g \left| \frac{1}{i\hbar}\hat{\mathrm{H}} \right| \psi \right\rangle = i\Omega^* c_e(t) \tag{1.16a}$$

$$\dot{c}_e = \langle e \,|\, \partial_t \,|\, \psi\rangle = \left\langle e \left| \frac{1}{i\hbar}\hat{\mathrm{H}} \right| \psi \right\rangle = i\Delta c_e(t) + i\Omega c_g(t). \tag{1.16b}$$

Assuming the atom to be initially in the ground state, the general solution to this set of equations is [19]

$$c_g(t) = e^{\frac{\Delta}{2}t}\left(\cos\left(\bar{\Omega}t\right) - i\frac{\Delta}{2\bar{\Omega}}\sin\left(\bar{\Omega}t\right)\right) \tag{1.17a}$$

$$c_e(t) = ie^{\frac{\Delta}{2}t}\frac{\Omega}{\bar{\Omega}}\sin\left(\bar{\Omega}t\right) \tag{1.17b}$$

with the *generalised Rabi frequency* $\bar{\Omega} = \sqrt{\Omega^2 + (\Delta/2)^2}$.

The qualitative response of the atom on the applied laser field depends on how close the laser is tuned to resonance, *i.e.* on the detuning. In the excitation scheme both resonant and off-resonant atomic response are used to efficiently excite atoms to the P-state; therefore, both cases need to be discussed here.

1.3.1 Resonant behaviour: Rabi oscillations

This system of equations has a particularly simple solution in the case of no detuning, *i.e.* $\Delta = 0$, assuming $|\psi(t=0)\rangle = |g\rangle$:

$$c_g(t) = \cos\left(|\Omega|t\right) \tag{1.18a}$$

$$c_e(t) = i\frac{\Omega}{|\Omega|}\sin\left(|\Omega|t\right) \tag{1.18b}$$

in which the population oscillates between $|g\rangle$ and $|e\rangle$, as shown in figure 1.5. These oscillations are called *Rabi oscillations* or *Rabi floppings*. They can be used to completely transfer the population from the ground- to the excited-state by applying a laser field for the time of a quarter oscillation period. By raising the applied laser intensity the Rabi frequency is increased and the time needed for a full population transfer is decreased.

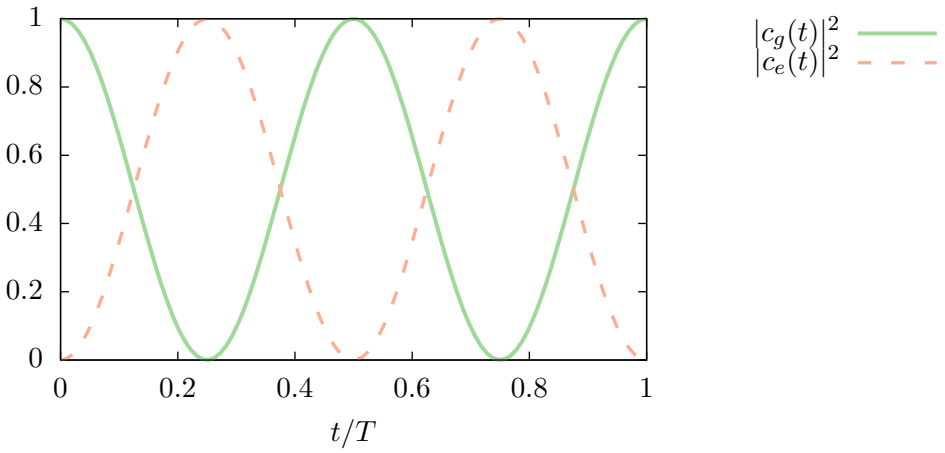

Figure 1.5: Rabi oscillations between ground- and excited-state: the time axis is given in units of $T = {}^{2\pi}/_{\Omega}$.

1.3.2 Off-resonant behaviour: AC-Stark shift

When the light field is far off-resonant with respect to the atomic transition, *i.e.* $|\Delta| \gg \Omega$, it does not induce oscillations between the states. Nevertheless, the atom is influenced by the light field as it causes the atomic levels to shift in energy. This energy shift can be derived in two different ways.

Adiabatic elimination: First it is assumed, that initially all the population is in the ground state. In the limit of a large detuning, *i.e.* $|\Delta| \gg \Omega$, most of the population stays in the ground state and the ground-state coefficient can be approximated as $c_g(t) \approx 1$. By inserting this into the differential equation for the excited-state coefficient (1.16b) a simple solution for its time evolution can be found [20]:

$$c_e(t) = -\frac{\Omega}{\Delta}\left(1 - \mathrm{e}^{i\Delta t}\right). \tag{1.19}$$

There are two terms: one constant term and one term that rapidly oscillates at frequency Δ. Over timescales larger than ${}^1/_{\Delta}$, this term averages to zero and in order to understand the slow dynamics of the system it can be neglected:

$$c_e(t) \approx -\frac{\Omega}{\Delta}. \tag{1.20}$$

Inserting (1.20) into the differential equation for the ground-state coefficient(1.16a) its differential equation becomes:

$$\dot{c}_g = -i\frac{|\Omega|^2}{\Delta}\, c_g. \tag{1.21}$$

Comparing this differential equation to the free time evolution of an isolated state $|\mathfrak{g}\rangle$ with an energy $E_\mathfrak{g} = \hbar\omega_\mathfrak{g}$ and a Hamiltonian for the free evolution $\hat{\mathrm{H}}_\mathfrak{g} = \hbar\omega_\mathfrak{g} |\mathfrak{g}\rangle \langle\mathfrak{g}|$:

$$\dot{c}_\mathfrak{g} = -i\omega_\mathfrak{g}\, c_\mathfrak{g} \tag{1.22}$$

it can be concluded that the ground state $|g\rangle$ off-resonantly coupled to $|e\rangle$ evolves in time as if it had an energy $\propto {}^{|\Omega|^2}/_{\Delta}$. This energy shift due to the applied light field is called *light shift* or *AC-Stark shift*. From a similar calculation under the assumption $c_e \approx 1$ it can be deduced that the excited state is shifted in the opposite direction by the same energy difference.

Dressed-state picture: The other way to understand these light induced shifts is to consider the change of the eigenstates due to atom-light coupling. The states $|g\rangle$ and $|e\rangle$ are eigenstates of the free Hamiltonian. It can be written in matrix form in the basis $|g\rangle = (1,0)^\mathrm{T}$, $|e\rangle = (0,1)^\mathrm{T}$ as

$$\hat{\mathrm{H}}_\mathrm{A} = \begin{pmatrix} 0 & 0 \\ 0 & \hbar\omega \end{pmatrix}. \tag{1.23}$$

Introducing interaction with a light field changes the total Hamiltonian to (1.10), which changes the off-diagonal elements in the matrix representation in the rotating frame and RWA:

$$\hat{\mathrm{H}} = -\hbar \begin{pmatrix} 0 & \Omega \\ \Omega^* & \Delta \end{pmatrix} \tag{1.24}$$

for which the two states $|g\rangle$ and $|e\rangle$ are no longer eigenstates. The new eigenstates of the full Hamiltonian are called *dressed states*, which in general are a superposition of $|g\rangle$ and $|e\rangle$:

$$|d_1\rangle = \frac{1}{N_1}\left(-\frac{\Delta + \sqrt{\Delta^2 + 4\Omega^2}}{2\Omega}\,|g\rangle + |e\rangle\right) \tag{1.25a}$$

$$|d_2\rangle = \frac{1}{N_2}\left(-\frac{\Delta - \sqrt{\Delta^2 + 4\Omega^2}}{2\Omega}\,|g\rangle + |e\rangle\right) \tag{1.25b}$$

where N_1 and N_2 are normalisation factors and Ω was assumed to be real. The new eigenenergies are:

$$E_1 = -\frac{\hbar}{2}\left(\Delta - \sqrt{\Delta^2 + 4\Omega^2}\right) \tag{1.26a}$$

$$E_2 = -\frac{\hbar}{2}\left(\Delta + \sqrt{\Delta^2 + 4\Omega^2}\right). \tag{1.26b}$$

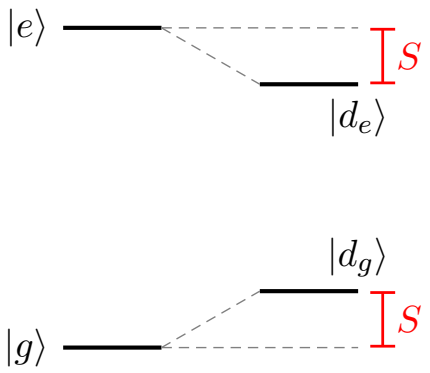

Figure 1.6: Energy shift of the atomic levels due to off-resonant light coupling by the AC-Stark shift S with $\Delta > 0$ in the far detuned limit $|\Delta| \gg \Omega$.

For a large detuning however, the off-diagonal elements in (1.24) are small compared to the diagonal elements and therefore the dressed states are approximately the old eigenstates with a small admixture of the other state:

$$|d_1\rangle \approx |d_g\rangle = \frac{1}{N_1'}\left(|g\rangle - \frac{\Omega}{\Delta}|e\rangle\right) \tag{1.27a}$$

$$|d_2\rangle \approx |d_e\rangle = \frac{1}{N_2'}\left(|e\rangle + \frac{\Omega}{\Delta}|g\rangle\right) \tag{1.27b}$$

with N_1', N_2' being the appropriate normalisation factors. The eigenenergies in this limit are:

$$E_g = 0 + \underbrace{\hbar\frac{\Omega^2}{\Delta}}_{S} \tag{1.28a}$$

$$E_e = -\hbar\Delta - \underbrace{\hbar\frac{\Omega^2}{\Delta}}_{S} \tag{1.28b}$$

which can be interpreted as the altered ground- and excited-state energies due to the AC-Stark shift S.

1.4 Incoherent phenomena

The four-level system under consideration involves the rapidly decaying excited state $|e\rangle$, as shown in figure 1.3. In order to account for the influence of this decay and to determine under which conditions it is relevant, a way to describe the effect of spontaneous emission is needed. Unfortunately, the simple approach of describing the system by Hermitian operators acting on Hilbert space vectors does not suffice and a different description is needed.

1.4.1 Density operator

Hilbert space vectors are one, but not the only, way to represent the state of a quantum system, and for many situations there are more useful ways to do it. In order to describe incoherent processes, such as spontaneous emission, the atom can be represented in terms of the *density operator* [21]

$$\hat{\rho} = \sum_i p_i \left|\psi_i\right\rangle \left\langle\psi_i\right| \tag{1.29}$$

where p_i denotes the probability of the atom to be in the quantum mechanical state $|\psi_i\rangle$. If there is a basis for which the density operator can be written as $\hat{\rho} = |\phi\rangle \langle\phi|$ for a single state vector $|\phi\rangle$ the system is said to be in a *pure state*. Else, it is said to be in a *mixed state*.

By inserting a complete set of states $\mathbb{1} = \sum_n |n\rangle \langle n|$ in some orthonormal basis $\{|n\rangle\}$ another way to represent the density operator can be found:

$$\hat{\rho} = \mathbb{1}\,\hat{\rho}\,\mathbb{1} = \sum_{n,m} \underbrace{\langle n \,|\, \hat{\rho} \,|\, m\rangle}_{\rho_{nm}} |n\rangle \langle m| \tag{1.30}$$

where ρ_{nm} is called the *density matrix*. The diagonal elements ρ_{nn} are called *populations* and denote the probabilities of finding the system in the basis state $|n\rangle$; whereas the off-diagonal elements are called *coherences*, which are a measure for the coherence of the superposition. It has to be noted that even though the density matrix and the density operator are different objects, these terms are often used interchangeably. Two important properties of the density operator are:

- $\hat{\rho} = \hat{\rho}^\dagger$ from which follows that $\rho_{ij} = {\rho_{ji}}^*$
- $\mathrm{Tr}[\hat{\rho}] := \sum_n \langle n \,|\, \hat{\rho} \,|\, n\rangle = \sum_n \rho_{nn} = 1$ which accounts for unitarity.

Furthermore the expectation value of a given operator $\hat{\mathrm{S}}$ can be written as

$$\left\langle \hat{\mathrm{S}} \right\rangle = \mathrm{Tr}\left[\hat{\rho}\hat{\mathrm{S}}\right]. \tag{1.31}$$

1.4.2 Master equation

In this subsection the differential equation governing the time evolution of the density operator (1.29) under the influence of spontaneous emission is presented; it is based on chapters 4.5 and 11.5 in D. Steck's *Quantum and Atom Optics* [16].

In general the time evolution of the density operator for a system described by a Hamiltonian $\hat{\mathrm{H}}$ is given by the *von-Neumann equation* [17]

$$\dot{\hat{\rho}} = \sum_i p_i \left(\underbrace{|\dot{\psi}_i\rangle}_{\frac{1}{i\hbar}\hat{\mathrm{H}}|\psi_i\rangle} \langle\psi_i| + |\psi_i\rangle \underbrace{\langle\dot{\psi}_i|}_{-\frac{1}{i\hbar}\hat{\mathrm{H}}\langle\psi_i|} \right) = \frac{1}{i\hbar}\left[\hat{\mathrm{H}}, \hat{\rho}\right]. \tag{1.32}$$

Spontaneous emission can be modelled by considering the atom to be coupled to a field of randomly fluctuating background radiation given by the Hamiltonian

$$\hat{\mathrm{H}} = \hat{\mathrm{H}}_\mathrm{S} + \hat{\mathrm{H}}_\mathrm{R} + \hat{\mathrm{H}}_\mathrm{SR} \tag{1.33}$$

where the total system, called the *universum*, is separated into the *system*—in this case the atom—and the *reservoir*—in this case the background radiation. $\hat{\mathrm{H}}_\mathrm{S}$ and $\hat{\mathrm{H}}_\mathrm{R}$ are the free system- and reservoir-Hamiltonians respectively, and $\hat{\mathrm{H}}_\mathrm{SR}$ describes the coupling between them. As the system is not isolated from its environment anymore, such systems are also called *open quantum systems*.

For the background radiation it can be assumed that the effect of the change of the system state on the reservoir state can be neglected. This means that it is assumed that the reservoir does not significantly change by the interaction with the atom. Such reservoirs are called *Markovian*. This is often referred to as the reservoir not having a memory of the previous interaction. One can include the effects of such a reservoir on the atom by an additional term in the equation of motion (1.32) [22]:

$$\dot{\hat{\rho}}_\mathrm{S} = \frac{1}{i\hbar}\left[\hat{\mathrm{H}}_\mathrm{S}, \hat{\rho}_\mathrm{S}\right] + \hat{\hat{\mathrm{L}}}\left[\hat{\rho}_\mathrm{S}\right] \tag{1.34}$$

where $\hat{\hat{\mathrm{L}}}\left[\hat{\rho}\right]$ is the *Lindblad superoperator* [23]. Equation (1.34) is called the *master equation*. It has to be noted that equation (1.34) is acting on the system density operator only, which can be obtained from the total density operator by tracing over the reservoir degrees of freedom:

$$\hat{\rho}_\mathrm{S} = \sum_r \langle r \,|\, \hat{\rho}_\mathrm{tot} \,|\, r\rangle = \mathrm{Tr}_\mathrm{R}\left[\hat{\rho}_\mathrm{tot}\right] \tag{1.35}$$

where the sum runs over a complete set of reservoir states $\{|r\rangle\}$. The explicit form of the Lindblad superoperator for spontaneous emission depends on the level structure of the atom. In general it can be written as

$$\hat{\hat{\mathrm{L}}}\left[\hat{\rho}_\mathrm{S}\right] = -\sum_k \frac{\gamma_k}{2}\left(\hat{\mathrm{L}}_k^\dagger \hat{\mathrm{L}}_k \hat{\rho}_\mathrm{S} + \hat{\rho}_\mathrm{S}\hat{\mathrm{L}}_k^\dagger \hat{\mathrm{L}}_k - 2\hat{\mathrm{L}}_k \hat{\rho}_\mathrm{S} \hat{\mathrm{L}}_k^\dagger\right) \tag{1.36}$$

where $\hat{\mathrm{L}}_k$ is the *Lindblad operator* for a given decay channel k.

For a simple two-level atom the terms in equation (1.33) are given from the *James-Cummings model* [24]

$$\hat{\mathrm{H}}_{\mathrm{S}} = -\hbar\Delta \left|e\right\rangle \left\langle e\right| \tag{1.37}$$

$$\hat{\mathrm{H}}_{\mathrm{R}} = \hbar \sum_j \left(\hat{\mathrm{a}}_j^\dagger \hat{\mathrm{a}}_j + \frac{1}{2}\right) \tag{1.38}$$

$$\hat{\mathrm{H}}_{\mathrm{SR}} = -\hbar \sum_j \left(g_j\, \hat{\mathrm{a}}_j \left|e\right\rangle \left\langle g\right| + g_j^* \hat{\mathrm{a}}_j^\dagger \left|g\right\rangle \left\langle e\right|\right) \tag{1.39}$$

where $\hat{\mathrm{a}}_j^\dagger, \hat{\mathrm{a}}_j$ are the creation and annihilation operators for the background radiation light field for different light field modes j, and g_j are the coupling constants between the modes and the atomic transition. In the zero temperature limit the master equation then reads:

$$\dot{\hat{\rho}}_{\mathrm{S}} = \frac{1}{i\hbar}\left[\hat{\mathrm{H}}_{\mathrm{S}}, \hat{\rho}_{\mathrm{S}}\right] - \frac{\gamma}{2}\left(\left|e\right\rangle \left\langle e\right| \hat{\rho}_{\mathrm{S}} + \hat{\rho}_{\mathrm{S}} \left|e\right\rangle \left\langle e\right| - 2\left|g\right\rangle \left\langle e\right| \hat{\rho}_{\mathrm{S}} \left|e\right\rangle \left\langle g\right|\right) \tag{1.40}$$

where γ is the spontaneous decay rate for decay from the excited- to the ground-state, for which the corresponding Lindblad operator is $\left|g\right\rangle \left\langle e\right|$.

If laser driving is included in the system Hamiltonian as in (1.15) the form of the Lindblad superoperator does not change under the assumption that the Rabi frequency is much smaller than the energy splitting between the two states, *i.e.* $\Omega \ll \omega$ [25]. This is true for all experimental situations that are considered here, as energy splittings are of the order of 100 THz whereas the Rabi frequencies are usually of the order of a few MHz. Hence, equation (1.40) also holds for system Hamiltonians of the form (1.15).

The additional Lindblad term in the von-Neumann equation effectively damps the off-diagonal elements of the density matrix and thereby reduces the coherence in the system. This means that an atom which is initially in a coherent superposition evolves to a completely incoherent superposition due to the interaction with the environment. Therefore, spontaneous emission is said to be a process of *decoherence*.

1.4.3 Optical Bloch equations

By projecting the master equation onto a given basis $\{\left|n\right\rangle\}$ one can obtain the differential equations for the density matrix in that basis:

$$\dot{\rho}_{nm} = \left\langle n \middle| \dot{\hat{\rho}} \middle| m \right\rangle. \tag{1.41}$$

For an n-level atom these, so called, *optical Bloch equations* (OBEs) are a set of $1/2(n^2+n)$ coupled differential equations. Together with the conditions

$$\rho_{nm} = \rho^*_{mn} \tag{1.42}$$

$$\sum_n \rho_{nn} = 1 \tag{1.43}$$

accounting for the Hermiticity of the density matrix and unitarity, these equations determine the time evolution of the density matrix.

For a laser driven two-level atom the optical Bloch equations are:

$$\dot{\rho}_{gg} = \gamma\rho_{ee} - i\Omega^*\rho_{eg} + i\Omega\rho_{ge} \tag{1.44a}$$

$$\dot{\rho}_{ee} = -\gamma\rho_{ee} + i\Omega^*\rho_{eg} - i\Omega\rho_{ge} \tag{1.44b}$$

$$\dot{\rho}_{ge} = -\frac{\gamma}{2}\rho_{ge} - i\Delta\rho_{ge} - i\Omega^*(\rho_{ee} - \rho_{gg}). \tag{1.44c}$$

The terms in the OBEs can be grouped according to different processes they are associated with: the terms with the Rabi frequency and detuning as prefactors determine the oscillatory behaviour of the populations; whereas the terms containing the decay rate cause population to be transferred from the excited- to the ground-state.

1.4.4 Finite laser linewidth

So far it was assumed that the atoms interact with a perfect single-mode light source. However, the lasers used for excitation in the experiment are not perfectly stable in frequency and may show a finite spectral width, also called linewidth, over the duration of the coupling to the system. The effect of this finite linewidth on the time evolution of the atom is to increase the damping of the off-diagonal density matrix elements, while not affecting the state populations [8, 26]. Therefore, the finite laser linewidth acts as an additional decoherence process, which can be modelled as an extra Lindblad term in the master equation (1.34):

$$\dot{\hat{\rho}}_S = \frac{1}{i\hbar}\left[\hat{\mathrm{H}}_S, \hat{\rho}_S\right] + \hat{\hat{\mathrm{L}}}\left[\hat{\rho}_S\right] + \hat{\hat{\mathrm{L}}}_{\text{laser}}\left[\hat{\rho}_S\right] \tag{1.45}$$

where $\hat{\hat{\mathrm{L}}}_{\text{laser}}$ accounts for the dephasing due to the finite laser linewidth. However, since laser linewidth for the lasers currently used in the experiment is only of the order of a few kHz, it is neglected throughout the rest of this thesis.

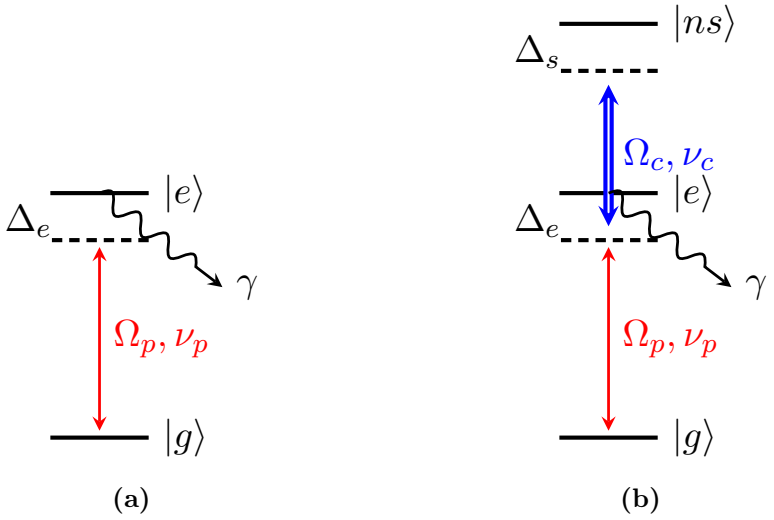

Figure 1.7: (a) Standard 2-level-system absorption, (b) 3-level EIT coupling scheme. The light fields are called *probe-* and *coupling-field*.

1.5 Electromagnetically induced transparency

Optical detection is one of the most precise imaging tools to observe dynamics in strongly interacting many-body quantum systems. Atoms in the ground state can usually be detected using the absorption imaging technique when a suitable closed cycled transition scheme is available. Being excited states with multiple decay channels, Rydberg atoms do not fulfil this requirement, and another method is needed to optically detect them. The imaging technique used in this experiment exploits the effect of electromagnetically induced transparency (EIT). In this section it is briefly outlined how EIT is induced in an ultracold gas.

Light with a frequency close to resonance of an atomic transition $|g\rangle \leftrightarrow |e\rangle$, as shown in figure 1.7a, propagating through an atomic medium of density ϱ experiences a complex susceptibility [8]

$$\chi(\nu_p) = \frac{\varrho|\mu_{eg}|^2}{\hbar\,\varepsilon_0}\frac{\rho_{eg}^{\mathrm{ss}}(\nu_p)}{\Omega_p} \tag{1.46}$$

where μ_{eg} is the dipole matrix element for the $|g\rangle \leftrightarrow |e\rangle$ transition, ε_0 is the vacuum permittivity, ρ_{eg}^{ss} denotes the steady-state solution to the coherence between $|g\rangle$ and $|e\rangle$, and ν_p is the light frequency. The susceptibility is linked to the optical properties of the atomic medium via the refractive index [8]

$$n = \sqrt{1+\chi} \approx 1 + \frac{\chi_{\mathrm{R}} + i\chi_{\mathrm{I}}}{2} \tag{1.47}$$

where χ_R and χ_I are the real and imaginary parts of the susceptibility respectively. The absorption of the medium is proportional to the imaginary part χ_I of the susceptibility; whereas the refraction is proportional to the real part χ_R.

In the following two cases are considered: absorption in a simple two-level system, as shown in figure 1.7a, and absorption in a three-level EIT-system where the excited state is additionally coupled to a metastable Rydberg state $|ns\rangle$, as depicted in figure 1.7b.

The steady-state solution for ρ_{eg} in a singly coupled system, as shown in figure 1.7a, is given by [27]:

$$\rho^{\mathrm{ss}}_{eg,2\mathrm{lvl}} = \frac{-i\Gamma_{ge}\Omega_p}{2|\Omega_p|^2 + |\Gamma_{ge}|^2}. \tag{1.48}$$

The steady-state solution for ρ_{eg} in a three-level system, as depicted in figure 1.7b, can be calculated from the optical Bloch equations for a three-level system:

$$\dot{\rho}_{gg} = +\gamma\rho_{ee} - i\Omega_p\rho_{ge} + i\Omega_p^*\rho_{eg} \tag{1.49a}$$

$$\dot{\rho}_{ee} = -\gamma\rho_{ee} + i\Omega_p\rho_{ge} - i\Omega_p^*\rho_{eg} - i\Omega_c\rho_{es} + i\Omega_c^*\rho_{se} \tag{1.49b}$$

$$\dot{\rho}_{ss} = +i\Omega_c\rho_{es} - i\Omega_c^*\rho_{se} \tag{1.49c}$$

$$\dot{\rho}_{ge} = -\underbrace{\left(\tfrac{\gamma}{2} + i\Delta_e\right)}_{\Gamma_{ge}}\rho_{ge} + i\Omega_p^*\left(\rho_{ee} - \rho_{gg}\right) - i\Omega_c\rho_{gs} \tag{1.49d}$$

$$\dot{\rho}_{gs} = -\underbrace{i\Delta_s}_{\Gamma_{gs}}\rho_{gs} + i\Omega_p^*\rho_{es} - i\Omega_c^*\rho_{ge} \tag{1.49e}$$

$$\dot{\rho}_{es} = -\underbrace{\left(\tfrac{\gamma}{2} + i\left(\Delta_s - \Delta_e\right)\right)}_{\Gamma_{es}}\rho_{es} + i\Omega_c^*\left(\rho_{ss} - \rho_{ee}\right) + i\Omega_p\rho_{gs} \tag{1.49f}$$

where γ denotes the decay rate of the rapidly decaying level $|e\rangle$, $\Delta_e = \nu_p - \omega_e$ and $\Delta_s = (\nu_p + \nu_c) - \omega_s$ are the n-photon detunings at levels $|e\rangle$ and $|s\rangle$ respectively, and Ω_p and Ω_c are the probe- and coupling-Rabi frequency respectively.

For EIT to occur, three conditions have to be met: the Rydberg state has to have a much smaller decay rate than the intermediate one, there should be no direct dipole allowed coupling between the ground- and the Rydberg-state and, finally, the coupling Rabi frequency needs to be much larger than the probe Rabi frequency, *i.e.* $\Omega_p \ll \Omega_c$.

In the steady state the density matrix does not change in time, and hence the time derivatives in (1.49) may be set to zero. Furthermore, since $\Omega_p \ll \Omega_c$, the population can be assumed to stay mostly in the ground state, *i.e.* $\rho_{gg} \approx 1$ [28]. The steady-state

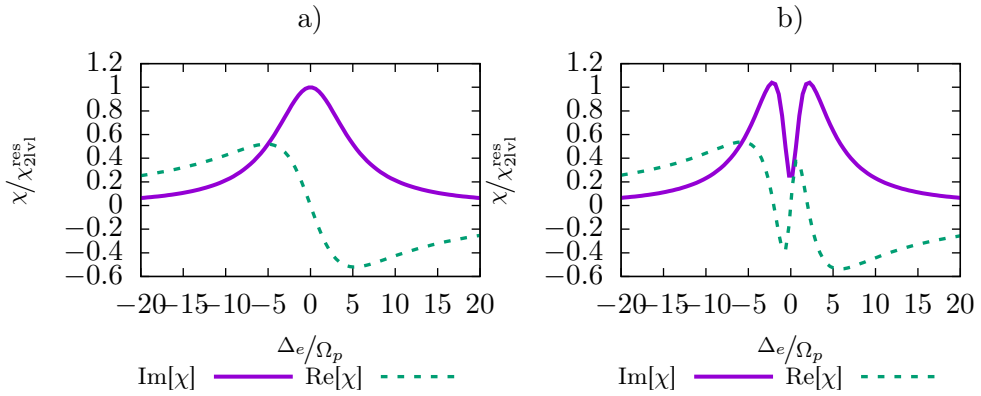

Figure 1.8: Absorption and refraction for two-level- (a) and three-level-absorbers (b) with $\Omega_c = 2\Omega_p$, $\gamma = 6\Omega_p$ and ν_c resonant on $|e\rangle \leftrightarrow |s\rangle$ transition, scaled by the two-level absorption at resonance $\chi^{\text{res}}_{\text{2lvl}}$

solution for ρ_{ge} is

$$\rho^{\text{ss}}_{ge} = \frac{-i\Omega_p}{\Gamma_{ge} + |\Omega_c|^2 \left(\Gamma_{gs} + \frac{|\Omega_p|^2}{\Gamma_{es}}\right)^{-1}} \tag{1.50}$$

from which ρ^{ss}_{eg} is given by $\rho^{\text{ss}}_{eg} = (\rho^{\text{ss}}_{ge})^*$.

In figure 1.8 the absorption and refraction for both cases are shown. For a two-level absorber, the absorption profile has the well-known Lorentzian shape. However, when the coupling laser is turned on, the medium is rendered transparent at the probe resonance. This effect is known as *electromagnetically induced transparency* (EIT) [28].

Chapter 2

Effective two-level description

As the four-level system is relatively complicated, there are many parameters needed in order to describe the dynamics: Ω_p, Ω_c, Ω_{mw}, Δ_e, Δ_s, Δ_p and γ. It is possible to use the master equation formalism, discussed in section 1.4, and generalise it to the four-level system, depicted in figure 1.3, to find the optical Bloch equations; in principle these would suffice to describe the excitation process of interest. However, the OBEs for such a system are a complicated set of coupled differential equations, as shown in the next chapter. On the one hand, because there is no general analytical solution, these OBEs have to be solved numerically. On the other hand, this set of OBEs is too complicated to yield an intuitive understanding of the excitation process. It would be preferable to have a simpler description in terms of fewer parameters.

In this chapter it is shown, that the excitation is performed in a regime for which the behaviour of the four-level system can be mainly described by only two effective parameters incorporating the complexity of the four-level dynamics. As the laser couplings in the four-level system are tuned far off resonance with respect to the intermediate levels, these states are only marginally populated. Therefore, the dynamics of the four-level system is expected to be dominated by the behaviour of the outer states $|g\rangle$ and $|p\rangle$. In the following it is shown, how the description of the four-level system can be simplified into an effective two-level description. This allows for an intuitive understanding of the system by thinking about the excitation dynamics in terms of the well-known two-level formulation.

To simplify things even further, first, the case of a two-photon/three-level excitation, as shown in figure 2.1a, is discussed. This case has been extensively studied in the context of Rydberg excitation of S- and D-states [9, 29–31]. Here, the laser couplings are also assumed to be tuned far off-resonance with respect to the intermediate level, neglecting the

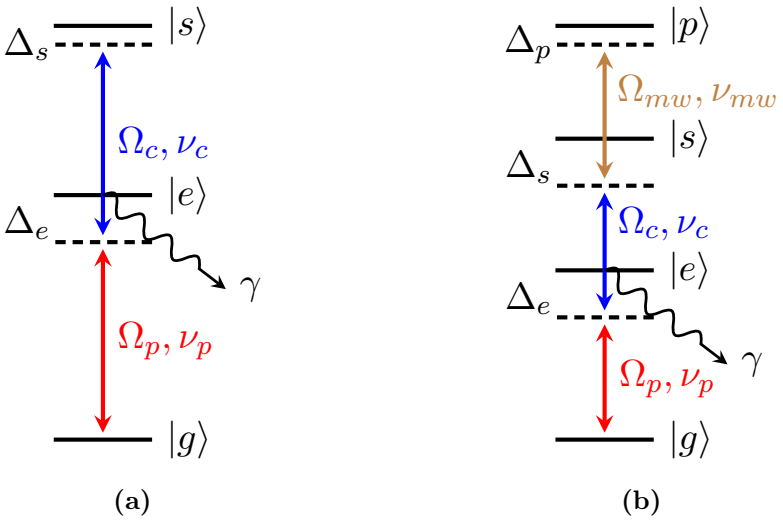

Figure 2.1: (a) Two-photon excitation level diagram. (b) Three-photon excitation level diagram.

influence of decay. Subsequently, this description is generalised to a three-photon/four-level excitation (figure 2.1b), and lastly the effects of the rapid decay of the excited state are discussed.

2.1 Two-photon excitation

When neglecting the decay of the intermediate level the density matrix formulation is not needed, and the system can be described in terms of a state vector

$$|\psi(t)\rangle = c_g(t)\,|g\rangle + c_e(t)\,|e\rangle + c_s(t)\,|s\rangle\,. \tag{2.1}$$

The Hamiltonian for such a system is given by the generalisation of equation (1.15) to the three-level case with two laser drivings

$$\begin{aligned}\hat{\mathrm{H}} = &-\hbar\Delta_e\,|e\rangle\langle e| - \hbar\Delta_s\,|s\rangle\langle s| \\ &-\hbar\left(\Omega_p\,|e\rangle\langle g| + \Omega_p^*\,|g\rangle\langle e|\right) \\ &-\hbar\left(\Omega_c\,|s\rangle\langle e| + \Omega_c^*\,|e\rangle\langle s|\right)\end{aligned} \tag{2.2}$$

which is given in the appropriate rotating frame and RWA. The detunings are defined as the respective n-photon detunings $\Delta_e := \nu_p - \omega_e$ and $\Delta_s := (\nu_p + \nu_c) - \omega_s$. The first two terms describe the free evolution of the atom; whereas the remaining terms describe the atom-light interaction in the semiclassical approach.

The set of differential equations governing the time evolution of the atomic state coefficients $c_i(t)$, $i \in \{g, e, s\}$, can easily be found using the Schrödinger equation

$$\dot{c}_g = \frac{1}{i\hbar} \left\langle g \middle| \hat{\mathrm{H}} \middle| \psi \right\rangle = i\Omega_p^* c_e \tag{2.3a}$$

$$\dot{c}_e = \frac{1}{i\hbar} \left\langle e \middle| \hat{\mathrm{H}} \middle| \psi \right\rangle = i\Delta_e c_e + i\Omega_p c_g + i\Omega_c^* c_s \tag{2.3b}$$

$$\dot{c}_s = \frac{1}{i\hbar} \left\langle s \middle| \hat{\mathrm{H}} \middle| \psi \right\rangle = i\Delta_s c_s + i\Omega_c c_e. \tag{2.3c}$$

For the three-level system, as in the four-level case, it is assumed that the laser couplings are tuned far off resonance with respect to the intermediate level $|e\rangle$, *i.e.* $|\Delta_e| \gg \Omega_p, \Omega_c, |\Delta_s|$. The effective two-level formulation of this three-level system is motivated by the observation that the time evolution of the system can be separated into two distinct timescales: the fast evolution of the intermediate state $|e\rangle$ and the slow evolution of the outer states $|g\rangle$ and $|s\rangle$. The intermediate population rapidly oscillates on the timescale given by the intermediate detuning $1/\Delta_e$. Assuming that the fast dynamics does not influence the dynamics on the slower timescale, it can be approximated that the intermediate state immediately reaches equilibrium, *i.e.* its time-derivative can be set to zero to lowest order in $\frac{\Omega_{p,c}}{\Delta_e}$ [20]:

$$c_e = -\frac{\Omega_p c_g + \Omega_c^* c_s}{\Delta_e}. \tag{2.4}$$

The intermediate population essentially adiabatically follows the time evolution of $|g\rangle$ and $|s\rangle$. This makes intuitively sense, as there is no resonant coupling to the intermediate state which could induce coherent population transfer. Furthermore, the intermediate state coefficient is suppressed by the small factors $\Omega_{p,c}/\Delta_e$ which agrees with the expected marginal population of this state.

Equation (2.4) can now be substituted back into equations (2.3) to find

$$\dot{c}_g = -i\frac{|\Omega_p|^2}{\Delta_e} c_g - i\frac{\Omega_p^* \Omega_c^*}{\Delta_e} c_s \tag{2.5a}$$

$$\dot{c}_s = i\left(\Delta_s - \frac{|\Omega_c|^2}{\Delta_e}\right) c_s - i\frac{\Omega_p \Omega_c}{\Delta_e} c_g \tag{2.5b}$$

where now the system can be expressed in terms of the ground- and S-state only. This procedure is called *adiabatic elimination*. This set of two coupled differential equations for the time evolution of the ground- and S-state can now be compared to the differential equations describing a two-level atom coupled to a single field (1.16). The terms coupling both differential equations together suggest the definition of the *effective Rabi frequency*

$$\Omega_{\text{eff}} := -\frac{\Omega_p \Omega_c}{\Delta_e}. \tag{2.6}$$

Moreover, there are additional prefactors for the free evolution of the ground- and excited-state evolution that can be identified as the AC-Stark shifts. However, the effective two-level system (2.5) differs from the real two-level system (1.16) as the Stark shifts in general do not have the same magnitude at both levels. Therefore, the AC-Stark shifts at levels $|g\rangle$ and $|s\rangle$ respectively are defined as:

$$S_g := \frac{|\Omega_p|^2}{\Delta_e} \tag{2.7}$$

$$S_s := \frac{|\Omega_c|^2}{\Delta_e} \tag{2.8}$$

which, together with (2.6), can be used to simplify the differential equations:

$$\dot{c}_g = -iS_g\, c_g + i\Omega_{\text{eff}}^*\, c_s \tag{2.9a}$$

$$\dot{c}_s = i\,(\Delta_s - S_s)\, c_s + i\Omega_{\text{eff}}\, c_g. \tag{2.9b}$$

By applying a transformation

$$c_{g,s} \longrightarrow c_{g,s}\, \mathrm{e}^{iS_g t} \tag{2.10}$$

which is equivalent to shifting the energy of the ground state by the amount of its AC-Stark shift, such that the ground-state energy becomes the zero-point energy again, the set of equations takes the form:

$$\dot{c}_g = i\Omega_{\text{eff}}^*\, c_s \tag{2.11a}$$

$$\dot{c}_s = i\Delta_{\text{eff}} c_s + i\Omega_{\text{eff}}\, c_g \tag{2.11b}$$

with the *effective detuning*

$$\Delta_{\text{eff}} := \Delta_s + S_g - S_s. \tag{2.12}$$

Comparing this to the set of differential equations for an off-resonant two-level atom (1.16), one finds that the system of the two states $|g\rangle$ and $|s\rangle$ behaves like a two-level atom with the substitutions $\Omega \longrightarrow \Omega_{\text{eff}}$ and $\Delta \longrightarrow \Delta_{\text{eff}}$, as depicted in figure 2.2a. From now on, the resonance of the bare states is called *two-photon resonance* and its detuning, the *two-photon detuning*, to be distinguished from the effective detuning and *effective resonance*.

Two important facts have to be noted at this point. Firstly, as the effective two-level

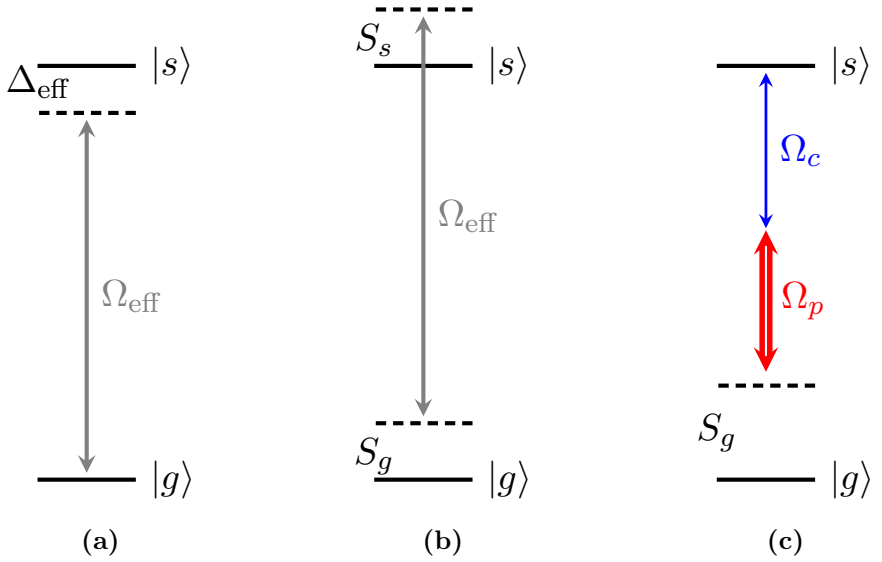

Figure 2.2: (a) effective two-level scheme (b) AC-Stark shifts S_g an S_s induced by laser couplings cancel each other out for $\Omega_p \approx \Omega_c$, where effective detuning Δ_{eff} coincides with two-photon detuning Δ_s ($= 0$ here) (c) for $\Omega_p \gg \Omega_c$ the ground-state Stark shift is dominant and the effective resonance is red shifted compared to the two-photon resonance

system in the form (2.11) follows exactly the same differential equations as the real two-level system, the analytical solution and the predictions for the behaviour on effective resonance and in the effectively off-resonant case, as discussed in section 1.3, can readily be adopted from the real two-level case. Secondly, the behaviour in this effective description depends solely on the two effective parameters; this substantially simplifies the understanding.

Assuming $\Omega_{\text{eff}} = \Omega_{\text{eff}}^*$ and initially having all the population in the ground state, the general solution to (2.11) can be copied from (1.17) [19]:

$$c_g(t) = e^{\frac{\Delta_{\text{eff}}}{2}t}\left(\cos\left(\bar{\Omega}_{\text{eff}}t\right) - i\frac{\Delta_{\text{eff}}}{2\bar{\Omega}_{\text{eff}}}\sin\left(\bar{\Omega}_{\text{eff}}t\right)\right) \tag{2.13a}$$

$$c_s(t) = ie^{\frac{\Delta_{\text{eff}}}{2}t}\frac{\Omega_{\text{eff}}}{\bar{\Omega}_{\text{eff}}}\sin\left(\bar{\Omega}_{\text{eff}}t\right) \tag{2.13b}$$

with $\bar{\Omega}_{\text{eff}} := \sqrt{\Omega_{\text{eff}}^2 + \left(\Delta_{\text{eff}}/2\right)^2}$ being the *generalised effective Rabi frequency.*

The effective detuning

$$\Delta_{\text{eff}} = \Delta_s + \frac{|\Omega_p|^2 - |\Omega_c|^2}{\Delta_e}. \tag{2.14}$$

can yield some insight into this effective system and contains two terms: the two-photon resonance and the difference between the AC-Stark shifts at both levels. This shows that in order to be on effective resonance not only must be the two-photon resonance fulfilled

but also the AC-Stark shifts have to cancel out (fig. 2.2b). The AC-Stark shifts cancelling out is equivalent to the condition $\Omega_p \approx \Omega_c$. Another possibility for being on the effective resonance is to have the two-photon resonance cancel out the difference in AC-Stark shifts, as shown in figure 2.2c. In other words: for given Rabi frequencies Ω_p and Ω_c, the effective resonance generally does not coincide with the two-photon resonance.

The amplitude of the Rabi oscillation of the probability to find the atom in the Rydberg-S-state is

$$P_{\max} = \max\left(|c_s(t)|^2\right) = \left|\frac{\Omega_{\text{eff}}}{\bar{\Omega}_{\text{eff}}}\right|^2 = \frac{\Omega_{\text{eff}}^2}{\Omega_{\text{eff}}^2 + \left(\Delta_{\text{eff}}/2\right)^2} \tag{2.15}$$

which means that in order to have full Rabi oscillations between both states the effective detuning has to be zero. Otherwise, some of the population is stuck in the ground state. Naively, one would expect that the higher one chooses one of the two Rabi frequencies the better the coupling between the ground- and Rydberg-S-state. But considering the effect of the probe- and coupling-Rabi frequencies on the amplitude through the effective detuning (2.14), one finds a rather surprising fact: the amplitude of the Rabi oscillations between $|g\rangle$ and $|s\rangle$ depends on the relative strength of the Rabi frequencies. This is due to the fact that if only one Rabi frequency is increased, an AC-Stark shift is introduced on one of the levels without being compensated by the other AC-Stark shift.

2.2 Three-photon excitation

The four-level system used for P-state excitation is very similar to the three-level system discussed in section 2.1, the only difference being having two intermediate levels that are far off resonance. In this section the method of adiabatic elimination, presented in section 2.1, is used to eliminate the intermediate levels in the four-level system. Furthermore a technique to find an effective master equation is presented to analyse the effects of spontaneous emission from the rapidly decaying excited state.

2.2.1 Adiabatic elimination

The four-level ladder-type system as shown in figure 2.1b, can be described in the appropriate rotating frame and RWA by the Hamiltonian

$$\begin{aligned}\hat{\mathrm{H}} = &-\hbar\Delta_e \left|e\right\rangle\left\langle e\right| - \hbar\Delta_s \left|s\right\rangle\left\langle s\right| - \hbar\Delta_p \left|p\right\rangle\left\langle p\right| \\ &- \hbar\left(\Omega_p \left|e\right\rangle\left\langle g\right| + \Omega_p^* \left|g\right\rangle\left\langle e\right|\right) \\ &- \hbar\left(\Omega_c \left|s\right\rangle\left\langle e\right| + \Omega_c^* \left|e\right\rangle\left\langle s\right|\right) \\ &- \hbar\left(\Omega_{mw} \left|p\right\rangle\left\langle s\right| + \Omega_{mw}^* \left|s\right\rangle\left\langle p\right|\right)\end{aligned} \tag{2.16}$$

with the *three-photon detuning* $\Delta_p := (\nu_p + \nu_c + \nu_{mw}) - \omega_p$. Neglecting the decay of the excited state for the moment, the general quantum state of the four-level system can be represented by the Hilbert-space state vector

$$\left|\psi(t)\right\rangle = c_g(t)\left|g\right\rangle + c_e(t)\left|e\right\rangle + c_s(t)\left|s\right\rangle + c_p(t)\left|p\right\rangle. \tag{2.17}$$

The differential equations governing the time evolution for the basis-state coefficients can be found by applying the Schrödinger equation using the Hamiltonian (2.16):

$$\dot{c}_g = \frac{1}{i\hbar}\left\langle g\right|\hat{\mathrm{H}}\left|\psi\right\rangle = i\Omega_p^* c_e \tag{2.18a}$$

$$\dot{c}_e = \frac{1}{i\hbar}\left\langle e\right|\hat{\mathrm{H}}\left|\psi\right\rangle = i\Delta_e c_e + i\Omega_p c_g + i\Omega_c^* c_s \tag{2.18b}$$

$$\dot{c}_s = \frac{1}{i\hbar}\left\langle s\right|\hat{\mathrm{H}}\left|\psi\right\rangle = i\Delta_s c_s + i\Omega_c c_e + i\Omega_{mw}^* c_p \tag{2.18c}$$

$$\dot{c}_p = \frac{1}{i\hbar}\left\langle p\right|\hat{\mathrm{H}}\left|\psi\right\rangle = i\Delta_p c_p + i\Omega_{mw} c_s. \tag{2.18d}$$

For large detunings at the intermediate levels, *i.e.* $|\Delta_e|, |\Delta_s| \gg \Omega_p, \Omega_c, \Omega_{mw}, |\Delta_p|$, for both intermediate state coefficients (2.18b) and (2.18c) two separate timescales appear: a fast evolution on the timescale of the detunings $1/\Delta_{e,s}$ and a slow evolution on the timescale of the Rabi frequencies $1/\Omega_{p,c,mw}$; this resembles the behaviour of the intermediate state for the three-level case. Assuming that the rapid oscillation does not influence the dynamics on the timescale of the Rabi frequencies, it can be approximated that the intermediate states instantaneously reach equilibrium; this assumption is further justified by numerically solving the full OBEs for this system in chapter 3. Therefore, similar to the three-level case, the time derivatives of the intermediate populations can be set to zero in first order to obtain:

$$c_e = -\frac{\Omega_p c_g + \Omega_c^* c_s}{\Delta_e} \tag{2.19a}$$

$$c_s = -\frac{\Omega_c c_e + \Omega_{mw}^* c_p}{\Delta_s}. \tag{2.19b}$$

The two intermediate states show a similar behaviour as the single intermediate state in the three-level case: both c_e and c_s adiabatically follow the evolution of the outer states $|g\rangle$ and $|p\rangle$. However, there is also a mixing term between both intermediate states induced by the coupling Rabi frequency Ω_c. The intermediate states also differ from the three-level case in the fraction of the population which is transferred into these states. Whereas the population of the intermediate state in the three-level case was effected by both outer states equally, here, the intermediate populations are mainly influenced by the coupling to the nearest outer state. The influence on the population by the nearest intermediate state can be ignored, as it is doubly suppressed, because the intermediate populations are already suppressed by factors of Ω_p/Δ_e and Ω_{mw}/Δ_s respectively.

Plugging equation (2.19a) into (2.19b) and vice versa one obtains

$$c_e = \left(1 - \frac{|\Omega_c|^2}{\Delta_e \Delta_s}\right)^{-1} \left(\frac{\Omega_c^* \Omega_{mw}^*}{\Delta_e \Delta_s}\, c_p - \frac{\Omega_p}{\Delta_e}\, c_g\right) \tag{2.20a}$$

$$c_s = \left(1 - \frac{|\Omega_c|^2}{\Delta_e \Delta_s}\right)^{-1} \left(\frac{\Omega_c \Omega_p}{\Delta_e \Delta_s}\, c_g - \frac{\Omega_{mw}^*}{\Delta_s}\, c_p\right) \tag{2.20b}$$

which can be used to eliminate c_e and c_s from equations (2.18) using the definition $\widetilde{\Delta}^2 := \Delta_e \Delta_s - |\Omega_c|^2$:

$$\dot{c}_g = -i \frac{\Delta_s |\Omega_p|^2}{\widetilde{\Delta}^2}\, c_g + i \frac{\Omega_p^* \Omega_c^* \Omega_{mw}^*}{\widetilde{\Delta}^2}\, c_p \tag{2.21a}$$

$$\dot{c}_p = i \left(\Delta_p - \frac{\Delta_e |\Omega_{mw}|^2}{\widetilde{\Delta}^2}\right) c_p + i \frac{\Omega_p \Omega_c \Omega_{mw}}{\widetilde{\Delta}^2}\, c_g \tag{2.21b}$$

where the *effective Rabi frequency* and *AC-Stark shifts* for the four-level case can be defined as

$$\Omega_{\text{eff}} := \frac{\Omega_p \Omega_c \Omega_{mw}}{\widetilde{\Delta}^2} \tag{2.22}$$

$$S_g := \frac{\Delta_s |\Omega_p|^2}{\widetilde{\Delta}^2} = \frac{|\Omega_p|^2}{\Delta_e - \frac{|\Omega_c|^2}{\Delta_s}} \tag{2.23}$$

$$S_p := \frac{\Delta_e |\Omega_{mw}|^2}{\widetilde{\Delta}^2} = \frac{|\Omega_{mw}|^2}{\Delta_s - \frac{|\Omega_c|^2}{\Delta_e}} \tag{2.24}$$

to simplify equations (2.21):

$$\dot{c}_g = -i S_g\, c_g + i \Omega_{\text{eff}}^*\, c_p \tag{2.25a}$$

$$\dot{c}_p = i\,(\Delta_p - S_p)\; c_p + i \Omega_{\text{eff}}\, c_g. \tag{2.25b}$$

With the altered Rabi frequency and Stark shifts, as defined above, the system is transformed into the same form as for the three-level atom after adiabatic elimination

(2.5). Hence, after setting the ground-state energy to to zero via the transformation $c_{g,p} \longrightarrow c_{g,p}\, e^{iS_g t}$, the set of differential equations can be copied from (2.11) [19]:

$$\dot{c}_g = i\Omega^*_{\text{eff}}\, c_p \tag{2.26a}$$

$$\dot{c}_p = i\Delta_{\text{eff}} c_p + i\Omega_{\text{eff}}\, c_g \tag{2.26b}$$

using the altered *effective detuning* $\Delta_{\text{eff}} := \Delta_p + S_g - S_p$. This, again, exactly matches the differential equations governing the behaviour of a real two-level atom (1.16). Hence, also in the four-level case, it possible to reduce the description of the four-level dynamics to the well-known two-level problem in the regime of large detunings at the intermediate states.

The solution to (2.26), with initially all the population in the ground state and assuming $\Omega_{\text{eff}} = \Omega^*_{\text{eff}}$, is given by (2.13)[1]. The explicit forms of the effective detuning and generalised effective Rabi frequency are:

$$\Delta_{\text{eff}} = \Delta_p + \frac{\Delta_s|\Omega_p|^2 - \Delta_e|\Omega_{mw}|^2}{\widetilde{\Delta}^2} \tag{2.27}$$

$$\bar{\Omega}_{\text{eff}} = \sqrt{\Omega^2_{\text{eff}} + \frac{1}{4}\left(\Delta_p + \frac{\Delta_s|\Omega_p|^2 - \Delta_e|\Omega_{mw}|^2}{\widetilde{\Delta}^2}\right)^2} \tag{2.28}$$

where here, in order for the effective detuning to vanish, not only the mere Rabi frequencies have to be taken into account but also the intermediate detunings. The Rabi frequencies are weighted by the more distant intermediate detuning. As before, the amplitude of the Rabi oscillation reads

$$P_{\max} = \max\left(|c_p(t)|^2\right) = \left|\frac{\Omega_{\text{eff}}}{\bar{\Omega}_{\text{eff}}}\right|^2 = \frac{\Omega^2_{\text{eff}}}{\Omega^2_{\text{eff}} + \left(\Delta_{\text{eff}}/2\right)^2} \tag{2.29}$$

which is the figure of merit when it comes to exciting P-states by driving three-photon Rabi oscillations from the ground state.

Neglecting the effects of decay, adiabatic elimination has reduced the rather complicated full description of the four-level dynamics to a very simple description characterised only by the effective parameters Ω_{eff} and Δ_{eff}.

2.2.2 Effects of the intermediate-state decay

Thus far, the effects of spontaneous emission have been neglected. As in the four-level scheme used for excitation the excited state $|e\rangle$ has a decay rate which is of the order of the used Rabi frequencies, it is expected to influence the excitation dynamics in a significant

[1] substituting $c_s(t) \longrightarrow c_p(t)$

way. In contrast to a real decaying two-level system, where the decay happens on the transition that is driven by the laser, here the decay happens on an intermediate state. Hence, it is expected that these two systems behave qualitatively differently.

A description of the system including spontaneous decay is needed in order to estimate whether or not the intermediate decay has a significant effect on the P-state excitation. This cannot be done in the simple description in terms of Hilbert-space vectors, used in the adiabatic elimination in 2.1 and 2.2.1; therefore, a density operator approach is used to include decoherence effects. Reiter and Sørensen have presented an *effective operator formalism for open quantum systems* (2012) [32] that is used here to derive an effective master equation to describe the excitation dynamics.

The basic idea is the same as for the adiabatic elimination performed on the atomic state coefficients $c_i(t)$: because the $|g\rangle \leftrightarrow |p\rangle$ transition is driven by lasers close to resonance and the lasers are off-resonant with respect to the intermediate levels $\{|e\rangle, |s\rangle\}$, the system dynamics separates into two different timescales: the slow evolution of $\{|g\rangle, |p\rangle\}$ and the rapidly oscillating evolution of $\{|e\rangle, |s\rangle\}$. Deviating from the notation in [32], here the states in subspace $\mathcal{O} = \{|g\rangle, |p\rangle\}$ are called *outer states*, whereas the states in $\mathcal{I} = \{|e\rangle, |s\rangle\}$ are called the *intermediate states*. The scheme used here eliminates the intermediate states and yields an effective description for the evolution of the outer states. The effective operator formalism is the equivalent of adiabatic elimination on the level of the master equation.

The Hilbert space can be separated into two orthogonal subspaces by the projection operators

$$\hat{\mathrm{P}}_{\mathcal{O}} := |g\rangle\langle g| + |p\rangle\langle p| \tag{2.30}$$

$$\hat{\mathrm{P}}_{\mathcal{I}} := |e\rangle\langle e| + |s\rangle\langle s| \tag{2.31}$$

with the properties $\hat{\mathrm{P}}_{\mathcal{O}} + \hat{\mathrm{P}}_{\mathcal{I}} = \mathbb{1}$ and $\hat{\mathrm{P}}_{\mathcal{O}}\hat{\mathrm{P}}_{\mathcal{I}} = 0$. They can be used to separate the Hamiltonian (2.16), describing the non-dissipative evolution of the laser-driven four-level system, into the two subspace Hamiltonians

$$\hat{\mathrm{H}}_{\mathcal{O}} := \hat{\mathrm{P}}_{\mathcal{O}}\hat{\mathrm{H}}\hat{\mathrm{P}}_{\mathcal{O}} = -\hbar\Delta_p |p\rangle\langle p| \tag{2.32}$$

$$\begin{aligned}\hat{\mathrm{H}}_{\mathcal{I}} :=& \hat{\mathrm{P}}_{\mathcal{I}}\hat{\mathrm{H}}\hat{\mathrm{P}}_{\mathcal{I}} \\ =& -\hbar\Delta_e |e\rangle\langle e| - \Delta_s |s\rangle\langle s| \\ & -\hbar\left(\Omega_c |s\rangle\langle e| + \Omega_c^* |e\rangle\langle s|\right)\end{aligned} \tag{2.33}$$

which only act on the respective subspace degrees of freedom. The connection between the two subspaces is given by the *excitations*

$$\hat{\mathrm{V}}_+ := \hat{\mathrm{P}}_{\mathcal{I}}\hat{\mathrm{H}}\hat{\mathrm{P}}_{\mathcal{O}} = -\hbar\Omega_p \left|e\right\rangle\left\langle g\right| - \hbar\Omega_{mw}^* \left|s\right\rangle\left\langle p\right| \tag{2.34}$$

and the *de-excitations*

$$\hat{\mathrm{V}}_- := \hat{\mathrm{P}}_{\mathcal{O}}\hat{\mathrm{H}}\hat{\mathrm{P}}_{\mathcal{I}} = -\hbar\Omega_p^* \left|g\right\rangle\left\langle e\right| - \hbar\Omega_{mw} \left|p\right\rangle\left\langle s\right| \tag{2.35}$$

that couple the outer- and intermediate-states, where $\hat{\mathrm{V}}_+^\dagger = \hat{\mathrm{V}}_-$ and $\hat{\mathrm{V}} := \hat{\mathrm{V}}_+ + \hat{\mathrm{V}}_-$. Hence, the total Hamiltonian (2.16) can be written as

$$\hat{\mathrm{H}} = \hat{\mathrm{H}}_{\mathcal{O}} + \hat{\mathrm{H}}_{\mathcal{I}} + \hat{\mathrm{V}}_+ + \hat{\mathrm{V}}_-. \tag{2.36}$$

In this formalism it is assumed that decay only occurs from the excited- to the ground-states. This is true for the system considered here, assuming the decay from the P-state is negligible. As shown in table 1.2, the timescale associated with the decay from the Rydberg-P- and Rydberg-S-states is much longer than the other timescales involved; thus it can safely be neglected. Since all other decay channels are either dipole forbidden or neglected, the only channel left is $\left|e\right\rangle \longrightarrow \left|g\right\rangle$ with a decay rate γ and its corresponding Lindblad operator $\hat{\mathrm{L}} = \left|g\right\rangle\left\langle e\right|$.

Defining a non-Hermitian Hamiltonian of the quantum jump formalism [32]:

$$\begin{aligned}\hat{\mathrm{H}}_{\mathrm{NH}} :=& \hat{\mathrm{H}}_{\mathcal{I}} - i\frac{\gamma}{2}\hat{\mathrm{L}}_k^\dagger\hat{\mathrm{L}}_k \\ =& -\hbar\,\delta_e \left|e\right\rangle\left\langle e\right| - \hbar\,\delta_s \left|s\right\rangle\left\langle s\right| \\ & -\hbar\left(\Omega_c \left|s\right\rangle\left\langle e\right| + \Omega_c^* \left|e\right\rangle\left\langle s\right|\right)\end{aligned} \tag{2.37}$$

where the detunings including decay are defined as $\delta_e := (\Delta_e + i\gamma/2)$, $\delta_s = \Delta_s$ and $\tilde{\delta}^2 := \delta_e\delta_s - |\Omega_c|^2$. The expression is non-Hermitian since $\delta_e^* \neq \delta_e$. The inverse of (2.37) with respect to the intermediate-state subspace identity $\mathbb{1}_{\mathcal{I}} = \left|e\right\rangle\left\langle e\right| + \left|s\right\rangle\left\langle s\right|$ is

$$\begin{aligned}\hat{\mathrm{H}}_{\mathrm{NH}}^{-1} =& -\frac{1}{\hbar}\frac{\delta_s}{\tilde{\delta}^2}\left|e\right\rangle\left\langle e\right| - \frac{1}{\hbar}\frac{\delta_e}{\tilde{\delta}^2}\left|s\right\rangle\left\langle s\right| \\ & + \frac{1}{\hbar}\frac{\Omega_c}{\tilde{\delta}^2}\left|s\right\rangle\left\langle e\right| + \frac{1}{\hbar}\frac{\Omega_c^*}{\tilde{\delta}^2}\left|e\right\rangle\left\langle s\right|.\end{aligned} \tag{2.38}$$

The effective Hamiltonian is given by [32]:

$$\begin{aligned}
\hat{\mathrm{H}}_{\mathrm{eff}} :=& -\frac{1}{2}\hat{\mathrm{V}}_{-}\left(\hat{\mathrm{H}}_{\mathrm{NH}}^{-1}+\left(\hat{\mathrm{H}}_{\mathrm{NH}}^{-1}\right)^{\dagger}\right)\hat{\mathrm{V}}_{+}+\hat{\mathrm{H}}_{\mathcal{O}} \\
=& \underbrace{+\frac{1}{2}\hbar\left(\frac{\delta_s|\Omega_p|^2}{\tilde{\delta}^2}+\frac{\delta_s|\Omega_p|^2}{\left(\tilde{\delta}^2\right)^*}\right)}_{\hbar S_g}|g\rangle\langle g| \\
&+\left(\underbrace{\frac{1}{2}\hbar\left(\frac{\delta_e|\Omega_{mw}|^2}{\tilde{\delta}^2}+\frac{\delta_e^*|\Omega_{mw}|^2}{\left(\tilde{\delta}^2\right)^*}\right)}_{\hbar S_p}-\hbar\Delta_p\right)|p\rangle\langle p| \\
&\underbrace{-\frac{1}{2}\hbar\left(\frac{\Omega_p\Omega_c\Omega_{mw}}{\tilde{\delta}^2}+\frac{\Omega_p\Omega_c\Omega_{mw}}{\left(\tilde{\delta}^2\right)^*}\right)}_{\hbar\Omega_{\mathrm{eff}}}|p\rangle\langle g| \\
&\underbrace{-\frac{1}{2}\hbar\left(\frac{\Omega_p^*\Omega_c^*\Omega_{mw}^*}{\tilde{\delta}^2}+\frac{\Omega_p^*\Omega_c^*\Omega_{mw}^*}{\left(\tilde{\delta}^2\right)^*}\right)}_{\hbar\Omega_{\mathrm{eff}}^*}|g\rangle\langle p|
\end{aligned} \tag{2.39}$$

where the prefactors can be identified as S_g and S_p being the AC-Stark shift at the ground- and P-state respectively and Ω_{eff} the effective Rabi frequency. These expressions can be rewritten using the identities

$$\frac{1}{2}\left(\frac{1}{\tilde{\delta}^2}+\frac{1}{\left(\tilde{\delta}^2\right)^*}\right)=\frac{\widetilde{\Delta}^2}{\widetilde{\Delta}^4+\left(\frac{\gamma\Delta_s}{2}\right)^2} \tag{2.40}$$

$$\frac{1}{2}\left(\frac{\delta_e}{\tilde{\delta}^2}+\frac{\delta_e^*}{\left(\tilde{\delta}^2\right)^*}\right)=\frac{\Delta_e\widetilde{\Delta}^2+\left(\frac{\gamma}{2}\right)^2\Delta_s}{\widetilde{\Delta}^4+\left(\frac{\gamma\Delta_s}{2}\right)^2}\approx\Delta_e\frac{\widetilde{\Delta}^2}{\widetilde{\Delta}^4+\left(\frac{\gamma\Delta_s}{2}\right)^2} \tag{2.41}$$

where in the last approximation it was used that $\gamma\ll|\Delta_e|,|\Delta_s|$:

$$S_g=\Delta_s|\Omega_p|^2\frac{\widetilde{\Delta}^2}{\widetilde{\Delta}^4+\left(\frac{\gamma\Delta_s}{2}\right)^2} \tag{2.42}$$

$$S_p=|\Omega_{mw}|^2\frac{\Delta_e\widetilde{\Delta}^2+\left(\frac{\gamma}{2}\right)^2\Delta_s}{\widetilde{\Delta}^4+\left(\frac{\gamma\Delta_s}{2}\right)^2}\approx\Delta_e|\Omega_{mw}|^2\frac{\widetilde{\Delta}^2}{\widetilde{\Delta}^4+\left(\frac{\gamma\Delta_s}{2}\right)^2} \tag{2.43}$$

$$\Omega_{\mathrm{eff}}=\Omega_p\Omega_c\Omega_{mw}\frac{\widetilde{\Delta}^2}{\widetilde{\Delta}^4+\left(\frac{\gamma\Delta_s}{2}\right)^2}. \tag{2.44}$$

These results are consistent with the expressions derived by adiabatic elimination on the state-vector coefficients, as they agree in the limit $\gamma \longrightarrow 0$, since

$$\frac{\widetilde{\Delta}^2}{\widetilde{\Delta}^4 + \left(\frac{\gamma\Delta_s}{2}\right)^2} \longrightarrow \frac{1}{\widetilde{\Delta}^2}. \tag{2.45}$$

In equation (2.39) the ground-state energy is shifted by the AC-Stark shift. In order to set the ground-state energy to zero again a unitary transformation $\hat{\mathrm{U}}(t) = e^{-iS_g t\,\mathbb{1}_{\mathcal{O}}} = e^{-iS_g t}\mathbb{1}_{\mathcal{O}}$ has to be applied to the system as in equation (1.12), where $\mathbb{1}_{\mathcal{O}} = |g\rangle\langle g| + |p\rangle\langle p|$ is the outer-state subspace identity. The transformed Hamiltonian is

$$\hat{\mathrm{H}}_{\mathrm{eff}} = -\hbar\underbrace{(\Delta_p + S_g - S_p)}_{\Delta_{\mathrm{eff}}}|p\rangle\langle p| - \hbar\left(\Omega_{\mathrm{eff}}|p\rangle\langle g| + \Omega^*_{\mathrm{eff}}|g\rangle\langle p|\right) \tag{2.46}$$

with the effective detuning

$$\Delta_{\mathrm{eff}} = \Delta_p + S_g - S_p = \Delta_p + \left(\Delta_s|\Omega_p|^2 - \Delta_e|\Omega_{mw}|^2\right)\frac{\widetilde{\Delta}^2}{\widetilde{\Delta}^4 + \left(\frac{\gamma\Delta_s}{2}\right)^2}. \tag{2.47}$$

Since, the detunings are the dominant frequencies in this system, the decay term is only a small correction to the denominator of (2.40), since $(\Delta_e\Delta_s - |\Omega_c|^2)^2 \gg {}^{(\gamma\Delta_s)^2}\!/_4$. Hence, the decay term can be treated as a small perturbation and (2.40) can be expanded in $\gamma\Delta_s$ around 0:

$$\frac{\widetilde{\Delta}^2}{\widetilde{\Delta}^4 + \left(\frac{\gamma\Delta_s}{2}\right)^2} = \frac{1}{\widetilde{\Delta}^2} - \frac{\gamma^2\Delta_s^2}{4\widetilde{\Delta}^6} + \mathcal{O}\left((\gamma\Delta_s)^3\right). \tag{2.48}$$

In the limit of large detunings already the first order correction term can be neglected for most purposes.

The effective Hamiltonian together with the effective Lindblad operator [32]

$$\begin{aligned}\hat{\mathrm{L}}_{\mathrm{eff}} &:= \hat{\mathrm{L}}\left(\hat{\mathrm{H}}_{\mathrm{NH}}\right)^{-1}\hat{\mathrm{V}}_+ \\ &= \underbrace{\frac{\delta_s\Omega_p}{\delta_e\delta_s - |\Omega_c|^2}}_{=:\alpha}|g\rangle\langle g| - \underbrace{\frac{\Omega_c^*\Omega_{mw}^*}{\delta_e\delta_s - |\Omega_c|^2}}_{=:\beta}|g\rangle\langle p|\end{aligned} \tag{2.49}$$

yields the effective master equation

$$\dot{\hat{\rho}} = \frac{1}{i\hbar}\left[\hat{\mathrm{H}}_{\mathrm{eff}}, \hat{\rho}\right] - \frac{\gamma}{2}\left(\hat{\mathrm{L}}^\dagger_{\mathrm{eff}}\hat{\mathrm{L}}_{\mathrm{eff}}\hat{\rho} + \hat{\rho}\hat{\mathrm{L}}^\dagger_{\mathrm{eff}}\hat{\mathrm{L}}_{\mathrm{eff}} - 2\hat{\mathrm{L}}_{\mathrm{eff}}\hat{\rho}\hat{\mathrm{L}}^\dagger_{\mathrm{eff}}\right) \tag{2.50}$$

that can be used to find the effective optical Bloch equations for the outer-state subspace density matrix ρ:

$$\dot{\rho}_{gg} = \gamma|\beta|^2\rho_{pp} + i\Omega^*_{\text{eff}}\rho_{pg} - i\Omega_{\text{eff}}\rho_{gp} - \frac{\gamma}{2}\alpha^*\beta\rho_{pg} - \frac{\gamma}{2}\beta^*\alpha\rho_{gp} \tag{2.51a}$$

$$\dot{\rho}_{pp} = -\gamma|\beta|^2\rho_{pp} - i\Omega^*_{\text{eff}}\rho_{pg} + i\Omega_{\text{eff}}\rho_{gp} + \frac{\gamma}{2}\alpha^*\beta\rho_{pg} + \frac{\gamma}{2}\beta^*\alpha\rho_{gp} \tag{2.51b}$$

$$\dot{\rho}_{gp} = -i\Delta_{\text{eff}}\rho_{gp} + i\Omega^*_{\text{eff}}\left(\rho_{pp} - \rho_{gg}\right) - \frac{\gamma}{2}\left(|\alpha|^2 + |\beta|^2\right)\rho_{gp} + \frac{\gamma}{2}\alpha^*\beta\left(\rho_{gg} + \rho_{pp}\right). \tag{2.51c}$$

These OBEs can now be compared to what would be expected from a real two-level atom with a decaying excited state (1.44). The terms in black resemble the master equation for a real two-level atom with the effective Rabi frequency (2.44), the effective detuning (2.47) and a decay rate

$$\widetilde{\gamma} = \gamma|\beta|^2 = \frac{\gamma|\Omega_c|^2|\Omega_{mw}|^2}{\widetilde{\Delta}^4 + \left(\frac{\gamma\Delta_s}{2}\right)^2} \tag{2.52}$$

where $\widetilde{\gamma} \ll \gamma$ because of the small prefactor, $|\beta|^2 \ll 1$, in the far off-resonant regime. The coloured terms, however, do not appear for real two-level atoms. The two scales for these terms are $\frac{\gamma}{2}\alpha^*\beta$, $\frac{\gamma}{2}\beta^*\alpha$ and $\frac{\gamma}{2}|\alpha|^2$. Both scales are real factors, assuming the Rabi frequencies are real, with

$$\Gamma := \frac{\gamma}{2}\alpha^*\beta = \frac{\gamma}{2}\beta^*\alpha = \frac{\gamma}{2}\frac{\Delta_s\Omega_p\Omega_c\Omega_{mw}}{\widetilde{\Delta}^4 + \left(\frac{\gamma\Delta_s}{2}\right)^2} \tag{2.53}$$

$$\Theta := \frac{\gamma}{2}|\alpha|^2 = \frac{\gamma}{2}\frac{\Delta_s^2\Omega_p^2}{\widetilde{\Delta}^4 + \left(\frac{\gamma\Delta_s}{2}\right)^2}. \tag{2.54}$$

Surprisingly, the extra terms act on the system as a reverse decay from the ground- to the P-state. The term $+\Gamma\left(\rho_{gg} + \rho_{pp}\right) \approx +\Gamma$ increases the coherence between the two states, which in turn, induces population transfer from the ground- to the P-state. This means that decay on the intermediate state may even enhance population transfer to the P-state. In the following, this is referred to as *intermediate decay enhanced population transfer*.

In the regime where the lasers are tuned far off resonance with respect to the intermediate levels, the timescale at which population is transferred to the P-state by this process is long compared to the period of the Rabi oscillation because $\Gamma \ll \Omega_{\text{eff}}$. Therefore, this process is expected to have little influence on the Rydberg P-state excitation in this regime. Going to smaller detunings this effect may play a bigger role; however, it is not possible to make reliable predictions for smaller detunings since the models presented here are only valid in the far off-resonant regime.

On timescales much shorter than $\widetilde{\gamma}$ and Γ the (downwards- or upwards-)decay of the P-state can be neglected and the behaviour of the system can again be approximated as an effective two-level system with an off-resonant Rabi frequency and oscillation amplitude:

$$\bar{\Omega}_{\text{eff}} = \sqrt{\Omega_{\text{eff}}^2 + \left(\Delta_{\text{eff}}/2\right)^2} \tag{2.55}$$

$$P_{\max} = \max\left(\left|c_p(t)\right|^2\right) = \frac{\Omega_{\text{eff}}^2}{\Omega_{\text{eff}}^2 + \left(\Delta_{\text{eff}}/2\right)^2} \tag{2.56}$$

where the intermediate decay leads to small corrections of the effective parameters Ω_{eff} and Δ_{eff}.

2.3 Other level structures and STIRAP

The method of adiabatic elimination of an off-resonantly coupled intermediate state, shown in 2.1 and 2.2.1, has been applied to ladder-type level schemes, as this way it is possible to address highly lying Rydberg states. However, in principle this method can be used for any kind of system, where intermediate states are bypassed by large detunings while resonantly coupling the outer states. The two other possibilities for a three-level scheme are shown in figure 2.3. For a four-level system there are a few more configurations, *e.g.* the N-type configuration [33]. The only difference in the calculations are the signs of the level energies and detunings.

Instead of resonantly coupling to the P-state in the four-level ladder-type system while being off-resonant with respect to the intermediate levels, it is also possible to have resonant coupling to all four states but have time dependent Rabi frequencies. In the *Stimulated Raman Adiabatic Passage* (STIRAP) the couplings are applied in a pulse sequence, where there are time delays between the pulses [34, 35]. Such schemes have

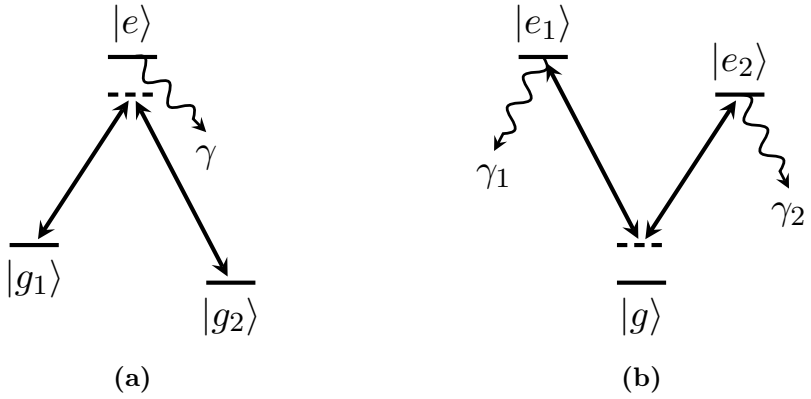

Figure 2.3: Other possible three-level configurations: (a) Λ-type with two ground states and one excited state, and (b) V-type with one ground state and two excited states

already been successfully implemented to excite Rydberg atoms in a three-level scheme [36]. A STIRAP scheme for the four-level ladder-type system has been proposed by Zhang *et al.* [37]. Their numerical simulations suggest that over 90% of the population may be transferred to the P-state in a STIRAP-pulse duration of a few 100 ns. However, the peak probe- and coupling-Rabi frequency used is 400 MHz which is far beyond the capabilities of the laser system currently used in the experiment.

Chapter 3

Numerical simulation of the four-level system

In order to check the validity of the effective models presented in chapter 2 and to understand the three-photon excitation scheme actually used in the experimental set-up, a full numerical simulation of the excitation, based on the optical Bloch equations, is carried out. This allows for simulating different excitation scenarios in great detail.

The master equation for a four-level system driven by three lasers as depicted in figure 2.1b is given by

$$\begin{aligned}\dot{\hat{\rho}} = &-\sum_k \frac{\gamma_k}{2}\left(\hat{\mathrm{L}}_k^\dagger \hat{\mathrm{L}}_k \hat{\rho} + \hat{\rho}\hat{\mathrm{L}}_k^\dagger \hat{\mathrm{L}}_k - 2\hat{\mathrm{L}}_k \hat{\rho} \hat{\mathrm{L}}_k^\dagger\right) \\ &+ \frac{1}{i\hbar}\left[\hat{\mathrm{H}}, \hat{\rho}\right] \end{aligned} \tag{3.1}$$

where the sum runs over the decay channels k. The decay channels and their respective decay rates γ_k and Lindblad operators $\hat{\mathrm{L}}_k$ are:

- $|p\rangle \longrightarrow |s\rangle$, γ_{ps}, $\hat{\mathrm{L}}_{ps} = |s\rangle\langle p|$
- $|s\rangle \longrightarrow |e\rangle$ γ_{se}, $\hat{\mathrm{L}}_{se} = |e\rangle\langle s|$
- $|p\rangle \longrightarrow |g\rangle$ γ_{pg}, $\hat{\mathrm{L}}_{pg} = |g\rangle\langle p|$
- $|e\rangle \longrightarrow |g\rangle$ γ_{eg}, $\hat{\mathrm{L}}_{eg} = |g\rangle\langle e|$.

Here all dipole-allowed decay channels are included; therefore, the implemented numerical scheme is generally able to include effects of all possible decays. However, for the analysis carried out in the rest of this chapter, only the rapid decay of the excited state, as shown in the schematic level structure in figure 2.1b, is considered.

The corresponding Hamiltonian is

$$\begin{aligned}\hat{\mathrm{H}} = &-\hbar\Delta_e \left|e\right\rangle\left\langle e\right| - \hbar\Delta_s \left|s\right\rangle\left\langle s\right| - \hbar\Delta_p \left|p\right\rangle\left\langle p\right| \\ &- \hbar\left(\Omega_p \left|e\right\rangle\left\langle g\right| + \Omega_p^* \left|g\right\rangle\left\langle e\right|\right) \\ &- \hbar\left(\Omega_c \left|s\right\rangle\left\langle e\right| + \Omega_c^* \left|e\right\rangle\left\langle s\right|\right) \\ &- \hbar\left(\Omega_{mw} \left|p\right\rangle\left\langle s\right| + \Omega_{mw}^* \left|s\right\rangle\left\langle p\right|\right)\end{aligned} \tag{3.2}$$

where, in general, the three-photon detuning $\Delta_p = (\nu_p + \nu_c + \nu_{mw}) - \omega_p$ at level $|p\rangle$ is included. From equations (3.1) and (3.2) the optical Bloch equations for the time evolution of the density matrix can be found by (1.41):

$$\dot{\rho}_{gg} = +\gamma_{eg}\rho_{ee} + \gamma_{pg}\rho_{pp} - i\Omega_p\rho_{ge} + i\Omega_p^*\rho_{eg} \tag{3.3a}$$

$$\dot{\rho}_{ee} = -\gamma_{eg}\rho_{ee} + \gamma_{se}\rho_{ss} + i\Omega_p\rho_{ge} - i\Omega_p^*\rho_{eg} - i\Omega_c\rho_{es} + i\Omega_c^*\rho_{se} \tag{3.3b}$$

$$\dot{\rho}_{ss} = -\gamma_{se}\rho_{ss} + \gamma_{ps}\rho_{pp} + i\Omega_c\rho_{es} - i\Omega_c^*\rho_{se} - i\Omega_{mw}\rho_{sp} + i\Omega_{mw}^*\rho_{ps} \tag{3.3c}$$

$$\dot{\rho}_{pp} = -\left(\gamma_{pg} + \gamma_{ps}\right)\rho_{pp} + i\Omega_{mw}\rho_{sp} - i\Omega_{mw}^*\rho_{ps} \tag{3.3d}$$

$$\dot{\rho}_{ge} = -\left(\tfrac{\gamma_{eg}}{2} + i\Delta_e\right)\rho_{ge} + i\Omega_p^*\left(\rho_{ee} - \rho_{gg}\right) - i\Omega_c\rho_{gs} \tag{3.3e}$$

$$\dot{\rho}_{gs} = -\left(\tfrac{\gamma_{se}}{2} + i\Delta_s\right)\rho_{gs} + i\Omega_p^*\rho_{es} - i\Omega_c^*\rho_{ge} - i\Omega_{mw}\rho_{gp} \tag{3.3f}$$

$$\dot{\rho}_{es} = -\left(\tfrac{\gamma_{se}}{2} + \tfrac{\gamma_{eg}}{2} + i\left(\Delta_s - \Delta_e\right)\right)\rho_{es} + i\Omega_c^*\left(\rho_{ss} - \rho_{ee}\right) + i\Omega_p\rho_{gs} - i\Omega_{mw}\rho_{ep} \tag{3.3g}$$

$$\dot{\rho}_{gp} = -\left(\tfrac{\gamma_{pg}}{2} + \tfrac{\gamma_{ps}}{2} + i\Delta_p\right)\rho_{gp} + i\Omega_p^*\rho_{ep} - i\Omega_{mw}^*\rho_{gs} \tag{3.3h}$$

$$\dot{\rho}_{ep} = -\left(\tfrac{\gamma_{eg}}{2} + \tfrac{\gamma_{pg}}{2} + \tfrac{\gamma_{ps}}{2} + i\left(\Delta_p - \Delta_e\right)\right)\rho_{ep} + i\Omega_p\rho_{gp} + i\Omega_c^*\rho_{sp} - i\Omega_{mw}^*\rho_{es} \tag{3.3i}$$

$$\dot{\rho}_{sp} = -\left(\tfrac{\gamma_{gs}}{2} + \tfrac{\gamma_{se}}{2} + \tfrac{\gamma_{pg}}{2} + i\left(\Delta_p - \Delta_s\right)\right)\rho_{sp} + i\Omega_{mw}^*\left(\rho_{pp} - \rho_{ss}\right) + i\Omega_c\rho_{ep} \tag{3.3j}$$

In the following section the implementation of the numerical simulation is explained and simulations are used to find the parameter range in which an effective two-level description is valid. This is followed by simulations of the experimental excitation schemes and a discussion of the consequences of the results.

3.1 Numerical integration scheme

The optical Bloch equations (3.3) are a set of 10 coupled differential equations, for which there is an additional constraint

$$\rho_{gg} + \rho_{ee} + \rho_{ss} + \rho_{pp} = 1 \tag{3.4}$$

ensuring unitarity [1]. Equations (3.3) can be written in terms of the diagonal and upper right off-diagonal elements of the density matrix ρ only, because the off-diagonal elements are coupled via the Hermiticity condition $\rho_{ij}^{*} = \rho_{ji}$. Therefore, the system has ten independent degrees of freedom in total.

To integrate the density matrix $\rho(t)$ forward in time according to the optical Bloch equations (3.3) the 4^{th} order Runge-Kutta method for solving ordinary linear differential equations is used [38]. Let $\vec{y}(t)$ be a vector containing the diagonal and the upper right off-diagonal elements of the density matrix, *i.e.*

$$\vec{y}(t) = \begin{pmatrix} \rho_{gg}(t) \\ \rho_{ee}(t) \\ \rho_{ss}(t) \\ \rho_{pp}(t) \\ \rho_{ge}(t) \\ \rho_{gs}(t) \\ \rho_{es}(t) \\ \rho_{gp}(t) \\ \rho_{ep}(t) \\ \rho_{sp}(t) \end{pmatrix} \tag{3.5}$$

where the optical Bloch equations can be expressed in the form

$$\dot{\vec{y}} = f\left(\vec{y}, t\right). \tag{3.6}$$

Furthermore, let $\Delta t > 0$ be the step size. $\vec{y}$ is integrated forward in time from a value at time t_n, $\vec{y}_n = \vec{y}(t_n)$, to a value at time $t_{n+1} = t_n + \Delta t$, $\vec{y}_{n+1} = \vec{y}(t_{n+1})$, by the formula:

$$\vec{y}_{n+1} = \vec{y}_n + \frac{\Delta t}{6}\left(\vec{k}_1 + 2\vec{k}_2 + 2\vec{k}_3 + \vec{k}_4\right) \tag{3.7}$$

where

$$\vec{k}_1 = f\left(t_n, \vec{y}_n\right) \tag{3.8a}$$

$$\vec{k}_2 = f\left(t_n + \tfrac{\Delta t}{2}, \vec{y}_n + \tfrac{\Delta t}{2}\vec{k}_1\right) \tag{3.8b}$$

$$\vec{k}_3 = f\left(t_n + \tfrac{\Delta t}{2}, \vec{y}_n + \tfrac{\Delta t}{2}\vec{k}_2\right) \tag{3.8c}$$

$$\vec{k}_4 = f\left(t_n + \Delta t, \vec{y}_n + \Delta t\,\vec{k}_3\right) \tag{3.8d}$$

are the intermediate increments. Unitarity is ensured by a normalisation constraint.

[1] Actually the OBEs already preserve unitarity; however, by this additional constraint small numerical errors may be corrected.

When simulating changes in the Rabi frequencies during the excitation process, the constant Rabi frequency parameters in the optical Bloch equations (3.3) are changed to time-dependent parameters

$$\Omega_p, \Omega_c, \Omega_{mw} \longrightarrow \Omega_p(t), \Omega_c(t), \Omega_{mw}(t). \tag{3.9}$$

3.2 Validity of the effective two-level description

By simulating the time evolution of the density matrix using the full optical Bloch equations, it can be checked to what extend and under which conditions the system behaves as an effective two-level system, as assumed in the previously discussed theory. The parameters chosen for the validity check of the two-level approximation are chosen such that they resemble the experimental conditions:

- $\Omega_p \approx 2\pi \times$ 1-10 MHz
- $\Omega_{mw} \approx 2\pi \times$ 1-10 MHz
- $\Omega_c \approx 2\pi \times 10\,\mathrm{MHz}$
- $\Delta_e = \Delta_s = -2\pi \times 100\,\mathrm{MHz}$
- $\gamma_{eg} = \gamma = 2\pi \times 6.067\,\mathrm{MHz}$
- $\gamma_{se}, \gamma_{pg}, \gamma_{ps} \approx 0$.

Figure 3.1 shows the time evolution for the atomic states under effective resonance without decay. The system behaves as one would expect from a two-level atom, undergoing full Rabi oscillations between $|g\rangle$ and $|p\rangle$. The intermediate populations are negligibly small compared to the populations in the outer states.

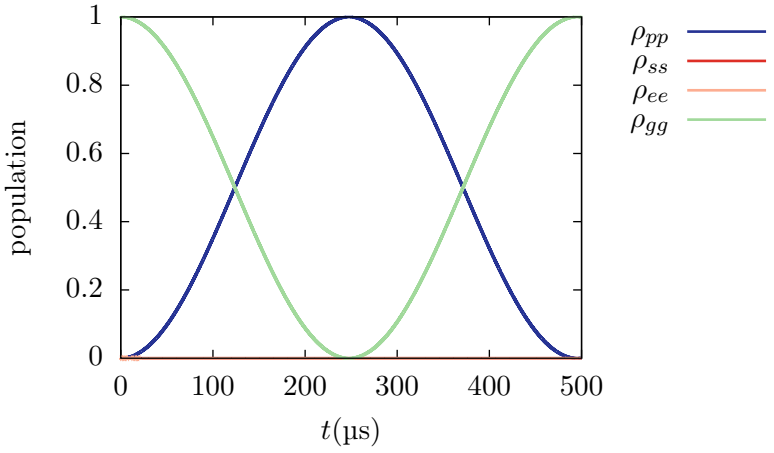

Figure 3.1: Simulation of the time-evolution of the atomic states under the conditions $\Delta_e = \Delta_s = -2\pi \times 100\,\mathrm{MHz}$, $\Omega_p = \Omega_{mw} = 2\pi \times 1\,\mathrm{MHz}$ $\Omega_c = 2\pi \times 10\,\mathrm{MHz}$, $\gamma = 0$ assuming all the population in the ground state initially. The intermediate populations are too small to be resolved in the plot. The effective parameters are: $\Delta_{\mathrm{eff}} = 0, \bar{\Omega}_{\mathrm{eff}} = 2\pi \times 1.01\,\mathrm{kHz}$.

In figure 3.2 the evolution of the excited-state population is shown for the same simulation. Here, two distinct timescales appear for the oscillation: one slow oscillation of the order of the effective Rabi frequency and one fast oscillation with a period $T_{\text{fast}} \approx 100\,\text{ns}$. The fast oscillation is due to to the term $\propto \Delta_e (= {}^{2\pi}/_{T_{\text{fast}}})$ in the differential equation for the excited-state population (2.18b). As assumed in the effective description, this fast oscillation indeed does not influence the dynamics on the slow timescale. Furthermore, the amplitude of this oscillation is small compared to the other amplitudes involved. The slow time evolution can be understood from equation (2.19a): neglecting the fast oscillation, the excited-state population roughly follows the ground-state population with a downscaled amplitude by the factor $-{}^{\Omega_p}/_{\Delta_e}$. The influence of the S-state population was neglected, as it is much smaller than the ground-state population.

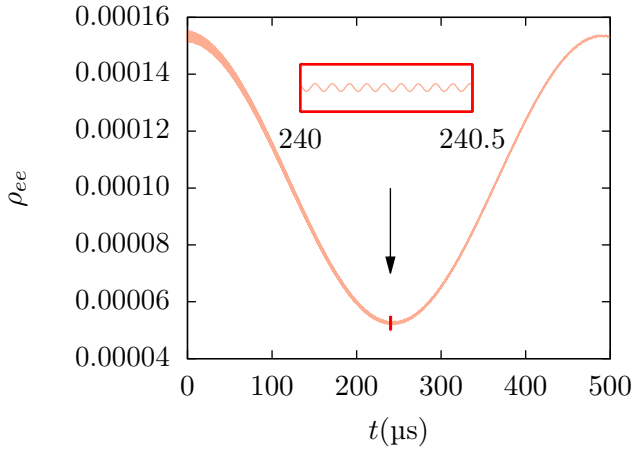

Figure 3.2: Simulation of the time-evolution of the excited-state population, parameters as in figure 3.1. The inlay shows the rapid oscillation on the timescale of the detuning ${}^{2\pi}/_{\Delta} = 100\,\text{ns}$.

The evolution of the S-state population, which is not plotted here, shows a similar behaviour: there is a fast oscillation which does not influence the oscillation on the timescale of the effective Rabi frequency; on this longer timescale the S-state population follows the P-state with a suppressed population.

The generalised Rabi frequency $\bar{\Omega}_{\text{eff}}$ and the amplitude of the Rabi oscillations between the ground- and P-state can be compared to its corresponding values in the full numerical simulations. This comparison can serve as a benchmark for how well the four-level system is described by the effective model. The quantity used to measure the deviation of $\bar{\Omega}_{\text{eff}}$ and P_{max} between the effective model and the simulation is the relative error

$$\left| \frac{x_{\text{model}} - x_{\text{sim}}}{x_{\text{model}}} \right| . \tag{3.10}$$

In figures 3.3 and 3.4 the relative errors of $\bar{\Omega}_{\text{eff}}$ and $P_{\max}$ for different values of Ω_p and Ω_{mw} are shown. All other parameters have been kept fixed.

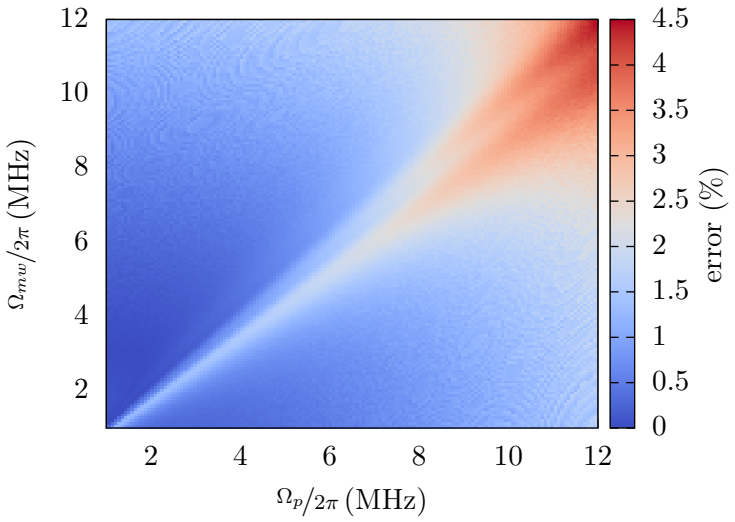

Figure 3.3: Relative error between the generalised Rabi frequency expected by the effective two-level description and the measured Rabi frequency in the full numerical simulation as a function of Ω_p, Ω_{mw}. The other parameters are as in figure 3.1, except for the decay rate which is set to $\gamma = 2\pi \times 6.067\,\text{MHz}$.

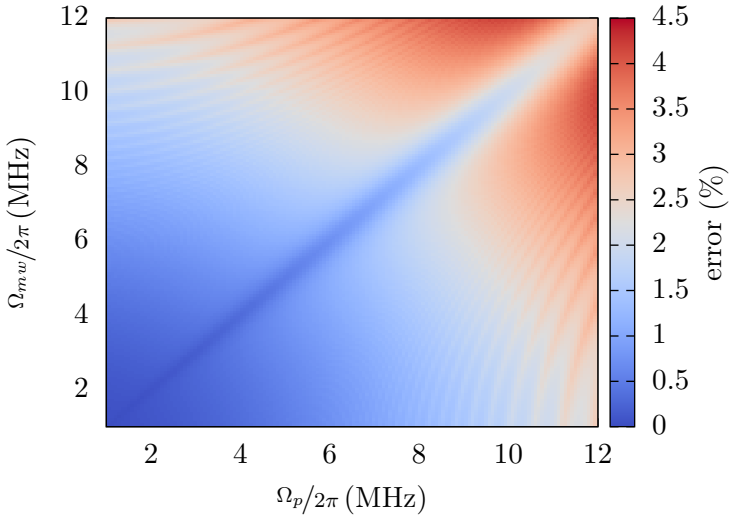

Figure 3.4: Relative error between the Rabi oscillation amplitude expected by the effective two-level description and the measured amplitude in the full numerical simulation as a function of Ω_p, Ω_{mw}. The other parameters are as in figure 3.1

For each data point in figure 3.3 a numerical simulation has been carried out in which the Rabi frequency of the P-state oscillation was measured. For most values of Ω_p and Ω_{mw} below $2\pi \times 5\,\text{MHz}$, which is the parameter range most relevant to the experiment, the relative error is well below 1%. However, on the effective resonance—in this case, where $\Omega_p \approx \Omega_{mw}$—the relative error is slightly higher but not exceeding 1.5%. This qualitative

behaviour also applies to the extended parameter range shown in the plot. It has to be noted that this scan does not cover Rabi frequencies smaller than $2\pi \times 1\,\mathrm{MHz}$ for Ω_p and Ω_{mw}, as the effective Rabi frequencies gets smaller which makes the simulation very time consuming. However, it was checked for fewer data points that this trend also continues for Rabi frequencies of $\approx 2\pi \times 0.1\,\mathrm{MHz}$, as expected.

In order to compare the amplitudes in the effective description and the full simulation, the decay was set to zero to not damp the oscillation. In the parameter range relevant for the experiment, the deviation is also well-below 1%; therefore, it can be concluded that the effective model reliably describes the four-level system in this parameter regime.

In both figures 3.3 and 3.4, the errors are large in parameter areas where the assumption $|\Delta_e|, |\Delta_s| \gg \Omega_p, \Omega_c, \Omega_{mw}, |\Delta_p|$ breaks down. As the effective descriptions only rely on one main assumption, it is simple to determine for which experimental situations it is valid.

Effects of the excited-state decay: The influence of excited-state decay is shown in figure 3.5. The oscillation between the ground- and P-state is damped and it approaches the value 0.5 as expected for a damped effective two-level system on resonance. The effective Rabi oscillation does not change significantly, as predicted.

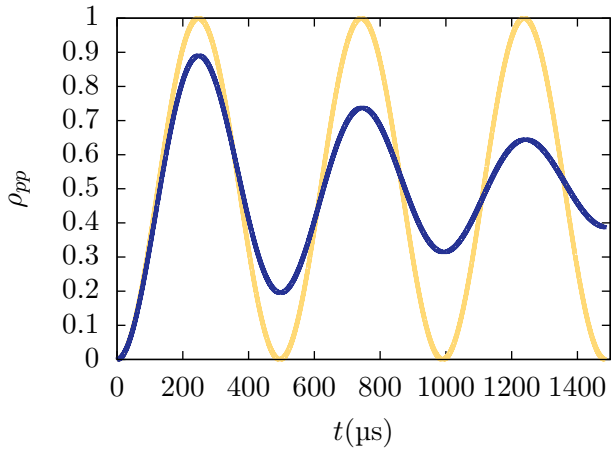

Figure 3.5: Simulation of the time-evolution of the P-state population with decay, $\gamma = 2\pi \times 6.067\,\mathrm{MHz}$, (blue line) and without decay (yellow line). Other parameters as in figure 3.1

The deviation from a real two-level system is revealed for a non-vanishing effective detuning, as shown in figure 3.6. The blue line shows the time-evolution of the P-state population for the four-level system compared to the evolution of the excited state in a real two-level system with decay on the excited state and a decay rate of $\gamma_{2\mathrm{lvl}} = \widetilde{\gamma} = \gamma|\beta|^2$ (yellow line). For the first period of the Rabi oscillation both curves show roughly the

same time evolution. Afterwards the effect of the intermediate decay enhanced population transfer to the P-state takes over. The transferred population exceeds the Rabi oscillation amplitude by far. Also the oscillation is damped on a timescale of about 100 µs whereas the timescale associated with $\widetilde{\gamma}$ is 20 ms. However, the deviation from the real two-level atom description does not mean that the effective two-level description is inaccurate, as the effects causing the deviation are described by the effective optical Bloch equations (2.51). In other words: the plots in figure 3.6 are the solutions to the effective optical Bloch equations with and without the terms that differ from a real two-level atom.

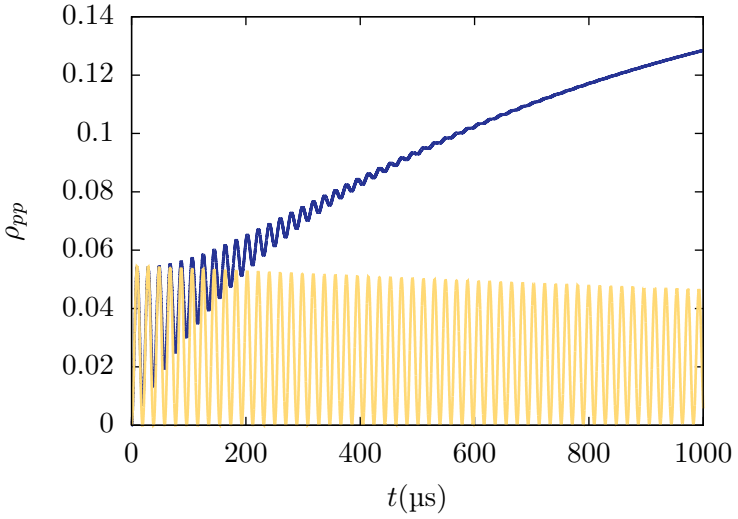

Figure 3.6: Comparison between an effective two-level atom with decay $\Delta_e = \Delta_s = -2\pi \times 100\,\text{MHz}$, $\Omega_p = 2\pi \times 2\,\text{MHz}$, $\Omega_{mw} = 2\pi \times 3\,\text{MHz}$ $\Omega_c = 2\pi \times 10\,\text{MHz}$, $\gamma = 2\pi \times 6.067\,\text{MHz}$, $\Delta_{\text{eff}} = -2\pi \times 0.0505\,\text{MHz}$, $\Omega_{\text{eff}} = 2\pi \times 0.006\,05\,\text{MHz}$, $\widetilde{\gamma} = 2\pi \times 0.000\,055\,\text{MHz}$, (blue line) and a real two-level atom with the effective parameters as two-level parameters, where the decay happens on the upper level (yellow line)

Three-level systems, as depicted in figure 2.1a, with a decay of the intermediate state show a similar behaviour [29].

The decay-enhanced population transfer can be understood by considering the dressed-state interpretation. The Hamiltonian (2.16) for the four-level system can be expressed in matrix form as:

$$\hat{\text{H}} = \hbar \begin{pmatrix} 0 & -\Omega_p & 0 & 0 \\ -\Omega_p & -\Delta_e & -\Omega_c & 0 \\ 0 & -\Omega_c & -\Delta_s & -\Omega_{mw} \\ 0 & 0 & -\Omega_{mw} & -\Delta_p \end{pmatrix} \tag{3.11}$$

where it was assumed that the Rabi frequencies are real numbers. Unfortunately, there is no analytical solution for the eigenenergies and eigenstates for general detunings and

Rabi frequencies. However, there is a solution for the special case $\Delta_p = 0, \Delta_e = \Delta_s =: \Delta$ and $\Omega_p = \Omega_{mw} =: \Omega$, for which the corresponding eigenenergies and eigenstates are:

$$E_1 = \hbar\omega_1 = \frac{\hbar}{2}\left(-\Delta + \Omega_c - \sqrt{4\Omega^2 + (\Delta - \Omega)^2}\right) \tag{3.12a}$$

$$E_2 = \hbar\omega_2 = \frac{\hbar}{2}\left(-\Delta - \Omega_c - \sqrt{4\Omega^2 + (\Delta + \Omega)^2}\right) \tag{3.12b}$$

$$E_3 = \hbar\omega_3 = \frac{\hbar}{2}\left(-\Delta + \Omega_c + \sqrt{4\Omega^2 + (\Delta - \Omega)^2}\right) \tag{3.12c}$$

$$E_4 = \hbar\omega_4 = \frac{\hbar}{2}\left(-\Delta - \Omega_c + \sqrt{4\Omega^2 + (\Delta + \Omega)^2}\right) \tag{3.12d}$$

$$|d_1\rangle = \frac{1}{N_1}\left(-|g\rangle + \frac{\omega_1}{\Omega}|e\rangle - \frac{\omega_1}{\Omega}|s\rangle + |p\rangle\right) \tag{3.13a}$$

$$|d_2\rangle = \frac{1}{N_3}\left(|g\rangle - \frac{\omega_2}{\Omega}|e\rangle - \frac{\omega_2}{\Omega}|s\rangle + |p\rangle\right) \tag{3.13b}$$

$$|d_3\rangle = \frac{1}{N_2}\left(-|g\rangle + \frac{\omega_3}{\Omega}|e\rangle - \frac{\omega_3}{\Omega}|s\rangle + |p\rangle\right) \tag{3.13c}$$

$$|d_4\rangle = \frac{1}{N_4}\left(|g\rangle - \frac{\omega_4}{\Omega}|e\rangle - \frac{\omega_1}{\Omega}|s\rangle + |p\rangle\right) \tag{3.13d}$$

where N_i are normalisation factors. This case corresponds to effective resonance as the Stark shifts at $|g\rangle$ and $|p\rangle$ are equal and thus cancel out. In the limit of large detunings, *i.e.* $|\Delta| \gg \Omega, \Omega_c$, the square root in the energy expressions can be approximated as $\approx \Delta$. Therefore, the dressed states separate into two classes: the two states $|d_1\rangle$, $|d_2\rangle$ with an energy $\approx -\hbar\Delta$, and the other two states $|d_3\rangle$, $|d_3\rangle$ with energies ≈ 0. In this limit the dressed states can be written as

$$|d_1\rangle \approx \frac{1}{\sqrt{2}}\left(|e\rangle - |s\rangle\right) \tag{3.14a}$$

$$|d_2\rangle \approx \frac{1}{\sqrt{2}}\left(|e\rangle + |s\rangle\right) \tag{3.14b}$$

$$|d_3\rangle \approx \frac{1}{N_2}\left(|g\rangle - |p\rangle\right) \tag{3.14c}$$

$$|d_4\rangle \approx \frac{1}{N_4}\left(|g\rangle + |p\rangle\right). \tag{3.14d}$$

However, for finite detunings all states have at least small contributions from all basis states $\{|g\rangle, |e\rangle, |s\rangle, |p\rangle\}$.

As the system moves away from effective resonance, the dressed states may only be found numerically, which is done in the following. For this, the following parameters are used: $\Delta_e = \Delta_s = -2\pi \times 100\,\text{MHz}$, $\Omega_c = 2\pi \times 10\,\text{MHz}$, $\Omega_p = 2\pi \times 1\,\text{MHz}$ and kept fixed while Ω_{mw} is changed, which thereby changes the effective detuning.

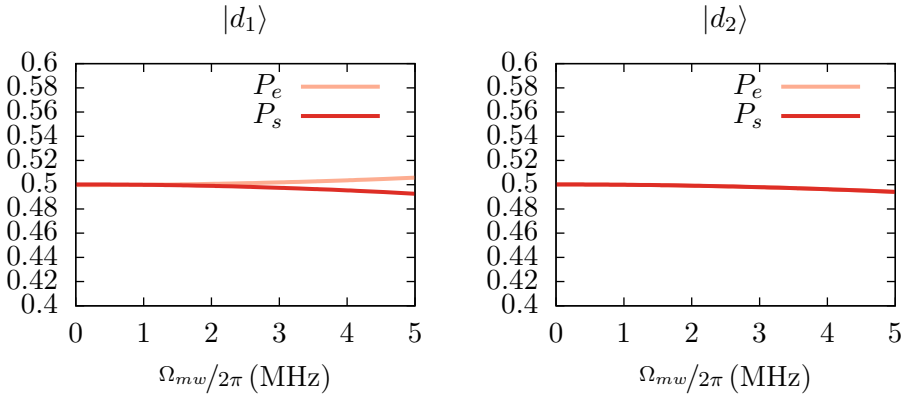

Figure 3.7: Excited- and S-state contributions of $|d_1\rangle$ and $|d_2\rangle$ expressed as probabilities $P_n(d_i) := |\langle n \,|\, d_i\rangle|^2$ as a function of microwave Rabi frequency

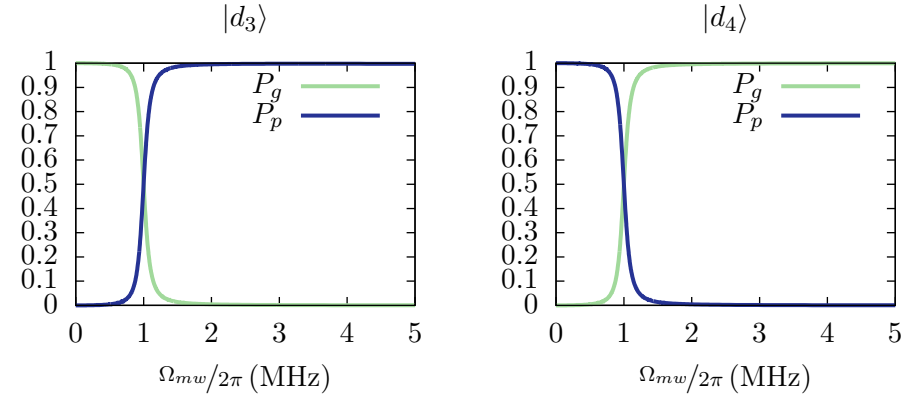

Figure 3.8: Ground- and P-state contributions of $|d_3\rangle$ and $|d_4\rangle$ expressed as probabilities $P_n(d_i) := |\langle n \,|\, d_i\rangle|^2$ as a function of microwave Rabi frequency

The dependence of the dressed states on the microwave Rabi frequency is shown in figures 3.7 and 3.8. The states $|d_1\rangle$ and $|d_2\rangle$ are not affected significantly, as their characteristics are expected to be dominated by the coupling between the excited- and S-state which is not changed here. Essentially, the two states remain the (anti-)symmetric superpositions (3.14a) and (3.14b). On the other hand, the two zero-energy dressed states change significantly with effective detuning. When $\Omega_{mw} < \Omega_p$, *i.e.* $\Delta_{\text{eff}} > 0$, $|d_3\rangle$ becomes essentially the ground state and $|d_4\rangle$ becomes the P-state and vice-versa for $\Delta_{\text{eff}} < 0$. At effective resonance, *i.e.* when $\Omega_p = \Omega_{mw}$, both states are in a superposition with equal contributions from the ground- and P-state, in agreement with the analytically derived dressed states.

A given state $|\psi(t)\rangle$ can be expressed in the basis of the dressed states as:

$$|\psi(t)\rangle = \sum_{i=0}^{4} c_i(t)\,|d_i\rangle\,. \tag{3.15}$$

As the states $|d_1\rangle$ and $|d_2\rangle$ contain large contributions of the rapidly decaying excited

state, c_1 and c_2 go to 0 on the timescale of the excited-state lifetime, assuming the population of the S-state is negligible. This leaves a superposition of $|d_3\rangle$ and $|d_4\rangle$.

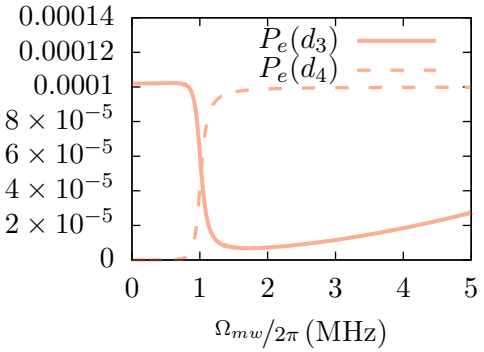

Figure 3.9: Excited-state contributions of $|d_3\rangle$ and $|d_4\rangle$ expressed as probabilities $P_n(d_i) := |\langle n\,|\,d_i\rangle|^2$ as a function of microwave Rabi frequency

As for finite detunings there is a non-zero excited state contribution to both $|d_3\rangle$ and $|d_4\rangle$, the excited state decay matters here as well. Figure 3.9 shows the excited state contribution as a function of Ω_{mw}. To understand the influence of the excited state decay, three cases have to be considered:

1. $\Omega_{mw} \approx \Omega_p$, $\Delta_{\text{eff}} \approx 0$: $P_e(d_3) \approx P_e(d_4)$
2. $\Omega_{mw} < \Omega_p$, $\Delta_{\text{eff}} > 0$: $P_e(d_3) > P_e(d_4)$
3. $\Omega_{mw} > \Omega_p$, $\Delta_{\text{eff}} < 0$: $P_e(d_3) < P_e(d_4)$

In the first case, the system is on effective resonance and both $|d_3\rangle$ and $|d_4\rangle$ have equal contributions of the decaying intermediate level, and $|\psi\rangle$ evolves into an equal superposition of these two dressed states. In the second case, as the excited state decays, the population is transferred into state $|d_4\rangle$, whereas it is transferred into state $|d_3\rangle$ in the third case. In both cases, the state in which the population is transferred to is $\approx |p\rangle$. Therefore, the intermediate decay transfers population from the ground- to the P-state when the system is effectively off-resonant. This contradicts the expectations from the predictions based on a non-decaying system. For a non-decaying system the mechanism by which population is transferred is the Rabi oscillation between the two states. For a system with intermediate decay, there is an additional transferring process which is the decay of a dressed state with a high contribution of the ground state.

In principle this process can be used to transfer population in a very robust way, if it were not for the finite lifetime of the Rydberg states. The timescale of this process can be estimated by the prefactor (2.53) associated with it in the effective optical Bloch

equations (2.51). Assuming $\Delta_e = \Delta_s = \Delta$ it can be written as

$$\Gamma \approx \frac{\gamma}{2}\frac{\Omega_{\text{eff}}}{\Delta}. \tag{3.16}$$

For typical parameters the effective Rabi frequency is of the order of a few 1 kHz to 10 kHz, whereas the detuning is of the order of 10 MHz to 100 MHz, therefore

$$\Gamma \approx 1 \times 10^{-5} \text{ to } 1 \times 10^{-3}\,\gamma. \tag{3.17}$$

So in order to make significant use of the intermediate decay enhanced population transfer in the regime where the lasers are tuned far off resonance with respect to the intermediate levels, one has to find a system in which the lifetimes of the rapidly decaying state and of the Rydberg state are a couple of orders of magnitude apart. Another possibility may be to decrease the detuning at the intermediate levels and thereby increase the effective Rabi frequency. However, this has to be further investigated as the models developed here are only valid in the far off-resonant regime, and therefore cannot make reliable predictions as the intermediate detunings are decreased.

3.3 Excitation scheme

The effective models and numerical simulations so far show that in principle it is possible to find a parameter regime for which the three-photon transition is on effective resonance, and the four-level system undergoes full Rabi-oscillations between the ground- and the P-state. Hence, the population can be completely transferred into the P-state by applying the lasers for the duration of a quarter Rabi cycle. However, for typical parameters the timescale of the Rabi oscillation is 10 µs to 1000 µs, whereas the typical lifetime of Rydberg states is ≈ 30 µs to 100 µs; depending on the chosen parameters, this can limit the population that can be transferred during one excitation cycle. Moreover, in order to be able to use the excited fraction of atoms to perform experiments on them, an excitation scheme with a duration of less than the Rydberg-state lifetime is desired.

The Rabi-pulse shape applied to the cold atoms sample is schematically depicted in figure 3.10. As the laser fields cannot be turned on and off instantaneously, the Rabi pulse is ramped up and down for a time τ_{ramp}. The pulse durations are of the order of 1 µs to 10 µs. The maximum Rabi frequencies $\Omega_{i,\text{max}}$ can be chosen independently for the three laser drivings.

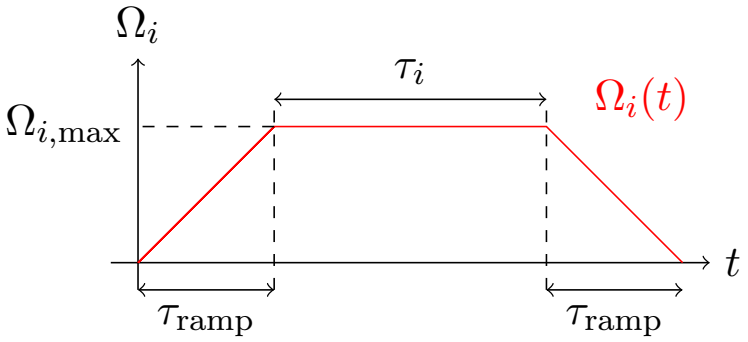

Figure 3.10: Excitation laser sequence, with a ramp-up time τ_{ramp}, a pulse duration τ_i and a maximum Rabi frequency $\Omega_{i,\max}$ for the applied fields Ω_i, $i \in \{p, c, mw\}$.

3.4 Excitation scheme optimisation

There are four parameters that can be changed in the excitation scheme: the maximum Rabi frequencies $\Omega_{i,\max}$ for the three pulses, *i.e.* $i \in \{p, c, mw\}$, the pulse duration τ; where fixed detunings and three-photon resonance, *i.e.* $\Delta_p = 0$, are assumed. As it is impractical to examine the dependence of all parameters simultaneously, the effect of changing each parameter is investigated separately. This obviously does not deliver the global optimum for the excitation process for a given parameter range but rather yields understanding for the influences of the different parameters on the excitation process. In turn, this understanding can serve as the basis for the actual excitation optimisation in the experiment.

The influence of changing the Rabi frequencies is shown in figure 3.11. The scans of the probe- and the microwave-Rabi frequency look very similar: as the Rabi frequency is increased, the population after the excitation shows oscillatory behaviour, where the maxima become smaller going to higher Rabi frequencies. The oscillation stems from the Rabi oscillation between the ground- and the P-state: as Ω_p or Ω_{mw} are changed, both the effective Rabi frequency (2.44) and the effective detuning (2.47) are changed which in turn change the generalised Rabi frequency (2.55). The oscillatory behaviour can be imagined as squeezing more and more Rabi oscillations into the fixed excitation window, as shown in figure 3.12.

The decrease of the maxima can be explained by the decrease of the Rabi oscillation amplitude: as Ω_p or Ω_{mw} are increased, the effective detuning is changed and according to equation (2.56) the amplitude of the Rabi oscillation changes. The expected Rabi oscillation amplitude is overplotted in figures 3.11a) and 3.11b). The amplitude reaches its maximum where $\Omega_p = \Omega_{mw}$, which corresponds to effective resonance as the intermediate detunings are equal. However, the maximum Rabi oscillation and the maximum population transfer achieved in the excitation cycle do not coincide. The reason for this

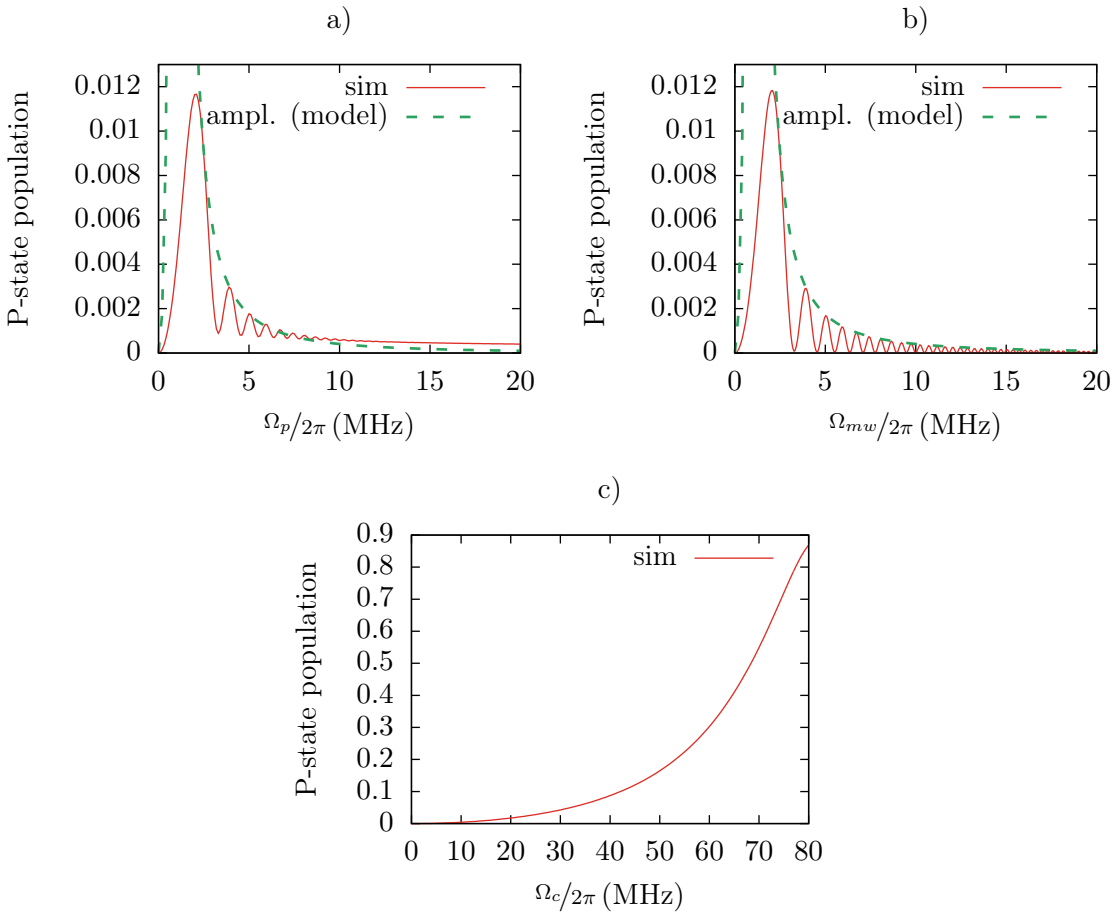

Figure 3.11: Simulated P-state population after excitation process as a function of a) Ω_p, b) Ω_{mw} and c) Ω_c (blue line) and Rabi oscillation amplitude from equation (2.56) (green line)

is that, for the parameters chosen here, at maximum Rabi oscillation the excitation time is shorter than a quarter of the oscillation period, *i.e.* the excitation is over before the P-state population reaches the maximum. By increasing either Ω_p or Ω_{mw}, the generalised Rabi frequency is also increased, and the P-state population at the end of the excitation cycle gets closer to the maximum of the oscillation. However, at the same time the amplitude is decreased. If the Rabi frequency of either Ω_p or Ω_{mw}, where the oscillation amplitude reaches is maximum, *i.e.* where the system is on effective resonance, is called Ω_{res}, and the Rabi frequency for which the period is such that the oscillation reaches the first maximum at the end of the excitation cycle is called Ω_{per}, the optimal Rabi frequency can be found between these two values, *i.e.*

$$\Omega_{\text{res}} < \Omega_{\text{opt}} < \Omega_{\text{per}}. \tag{3.18}$$

From a naive point of view, the fact that the excitation becomes less efficient when increasing either of these two Rabi frequencies above a certain threshold is surprising. One

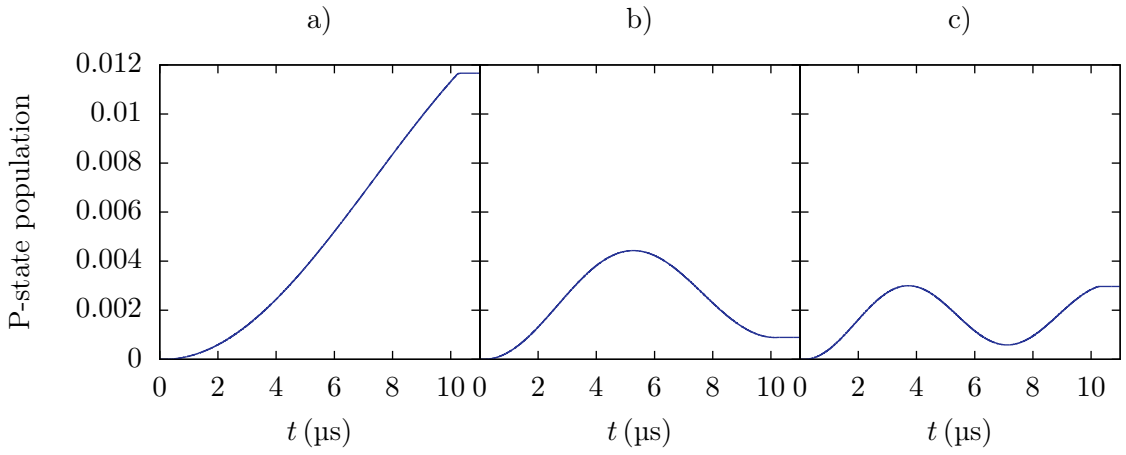

Figure 3.12: Time evolution of the P-state population during one excitation cycle. The parameters used are: a) as for the 1st maximum in fig. (3.11a), b) as for the 1st minimum in fig. (3.11a) and c) as for the 2nd maximum in fig. (3.11a).

would rather expect to enhance population transfer by increasing one of the couplings. However, one has to consider the effect of the AC-Stark shifts which shift the system out of effective resonance and thereby reduce the excitation efficiency. The most important experimental consequence is that the microwave coupling has to be adjusted carefully. As the S- and P-state are Rydberg states with a high principal quantum number, the dipole matrix element corresponding to the $|s\rangle \leftrightarrow |p\rangle$ transition is orders of magnitude larger compared to those for transitions between states with low principal quantum numbers. As the Rabi frequency is proportional to the dipole matrix element, even moderate intensities for the microwave field can lead to Rabi frequencies which are orders of magnitude larger than the probe Rabi frequency which in turn significantly reduces the population transfer in the excitation.

The expression (2.56) for the oscillation amplitude is only valid for timescales much shorter than $\widetilde{\gamma}$ and Γ, where the decay terms in the effective optical Bloch equations (2.51) can be neglected. In figure 3.11a) it can be seen that for high probe Rabi frequencies the transferred population in the numerical simulation exceeds the calculated Rabi oscillation amplitude. This is due to enhanced population transfer by the intermediate decay. Figure 3.12c) shows the same effect: at the first minimum of the P-state oscillation the population does not vanish but shows an offset caused by the population that has been transferred by upwards decay.

Although they are not resolved in the plot, the effects of upwards decay are also present in the scan of the microwave Rabi frequency in figure 3.11b). The effects are not as

pronounced as in the probe Rabi frequency scan, because a high probe coupling increases the excited-state population and thereby the influence of its decay.

Nevertheless, the dominant process by which population is transferred in this parameter regime is the Rabi oscillation between the ground- and the P-state. The effect of upwards decay plays only a minor role.

The coupling Rabi frequency dependence of the excited-state population after excitation, shown in figure 3.11c), does not show an oscillatory behaviour, because the coupling strength changes the effective parameters differently: the coupling Rabi frequency enters only in the scaling factor of the effective detuning (2.47) and therefore changes it more slowly compared to the probe- or microwave-Rabi frequency. The plot shows that increasing the coupling Rabi frequency is beneficial to the population transfer. The currently used laser system is run at a coupling Rabi frequency of around $2\pi \times 10\,\mathrm{MHz}$ which can be further increased to around $2\pi \times 25\,\mathrm{MHz}$.

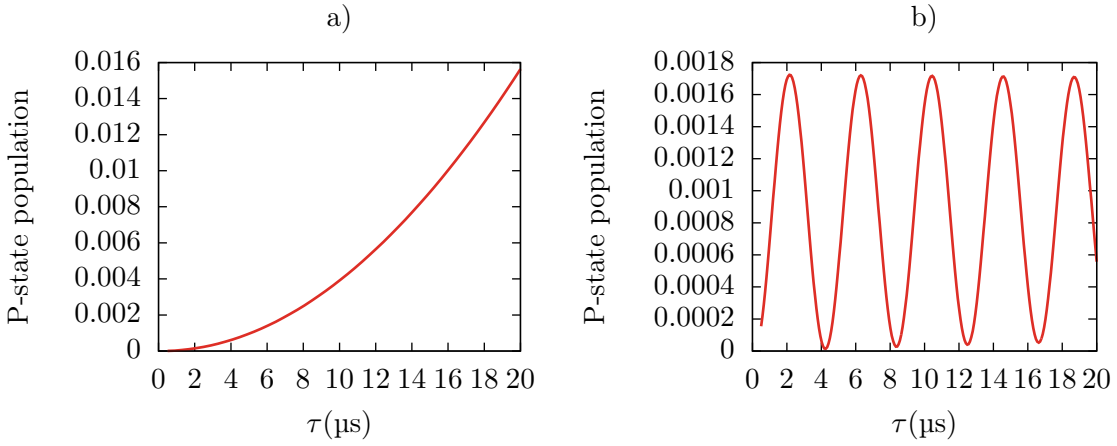

Figure 3.13: Simulated P-state population after excitation process as a function pulse duration τ: a) on effective resonance and b) effectively off-resonant.

The influence of the pulse duration on the excitation is rather trivial: it increases the time in which the system can undergo oscillations between ground- and P-state. In the parameter range investigated here, this means that on effective resonance, where a quarter oscillation period is larger than the pulse duration, the population transfer is increased because the population can evolve closer to the oscillation maximum before the pulse is over (fig. 3.13a)). For a system which is effectively off resonance with an oscillation period which is comparable to or smaller than the pulse duration, the pulse duration determines how many Rabi oscillations the system undergoes before the end of the excitation (fig. 3.13b)). As the population transfer is more efficient close to effective resonance a longer pulse duration would be preferable. However, the finite lifetime of the Rydberg P-state of $\approx 50\,\mu\mathrm{s}$ (for the 42P-state [12]) limits the maximum pulse duration. In order to perform experiments using the atoms which have been excited to the P-state,

the excitation process needs to be shorter than the lifetime; therefore a pulse duration of 10 µs is suggested.

So far, all simulations have been carried out in a regime where the half period of the effective two-level Rabi oscillation on effective resonance is longer than the excitation cycle. In order to check what the highest reachable population transfers are, simulations close to the experimentally highest achievable Rabi frequencies have been done. As in figure 3.14a) can be seen, population transfers of over 90% can be reached. The reason the system is not undergoing full Rabi oscillations is the approaching breakdown of the two-level regime for higher Rabi frequencies.

In figure 3.14 the effective resonance was achieved by setting the probe- and microwave-Rabi frequency equal and thereby ensuring that the AC-Stark shifts at $|g\rangle$ and $|p\rangle$ cancel out. However, the effective model shows that the effective resonance can also be achieved by counteracting the difference in AC-Stark shifts with the three-photon detuning Δ_p, as it is shown in figure 3.14b). This is particularly interesting when the laser system has different maximum Rabi frequencies for the different couplings. Thereby the maximum laser intensity on all couplings can be used without sacrificing population transfer by inducing an effective detuning.

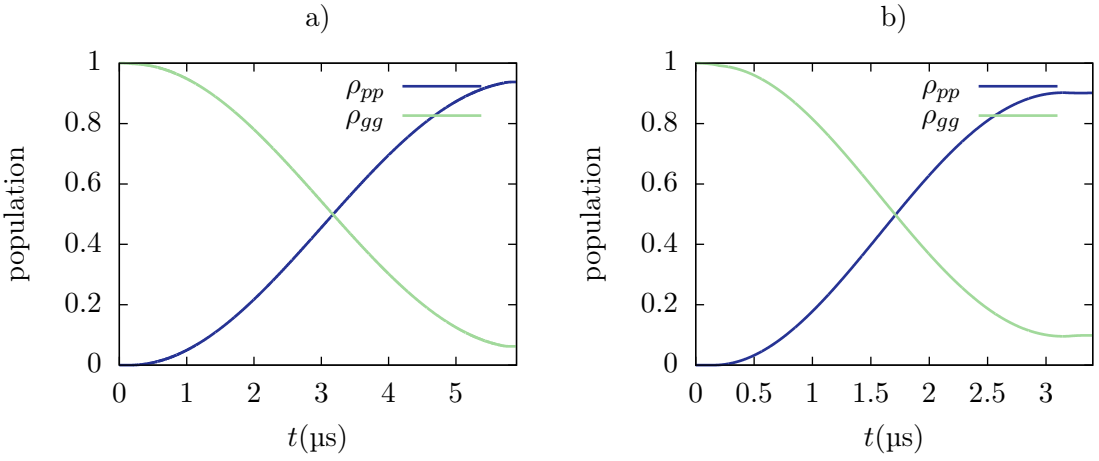

Figure 3.14: Excitation close to maximum Rabi frequencies: a) with cancelling AC-Stark shifts, where $\Omega_p = \Omega_{mw} = 2\pi \times 4\,\text{MHz}$, $\Omega_c = 2\pi \times 25\,\text{MHz}$, $\Delta_e = \Delta_s = -2\pi \times 100\,\text{MHz}$, $\Delta_p = 0$ b) with three-photon detuning cancelling difference in AC-Stark shifts, where $\Omega_p = 2\pi \times 8\,\text{MHz}$, $\Omega_{mw} = 2\pi \times 4\,\text{MHz}$, $\Omega_c = 2\pi \times 25\,\text{MHz}$, $\Delta_e = \Delta_s = -2\pi \times 100\,\text{MHz}$, $\Delta_p = 2\pi \times 0.511\,\text{MHz}$ such that $\Delta_{\text{eff}} = 0$. The excitation durations where adjusted to $\approx {}^{2\pi}/_{\Omega_{\text{eff}}}$

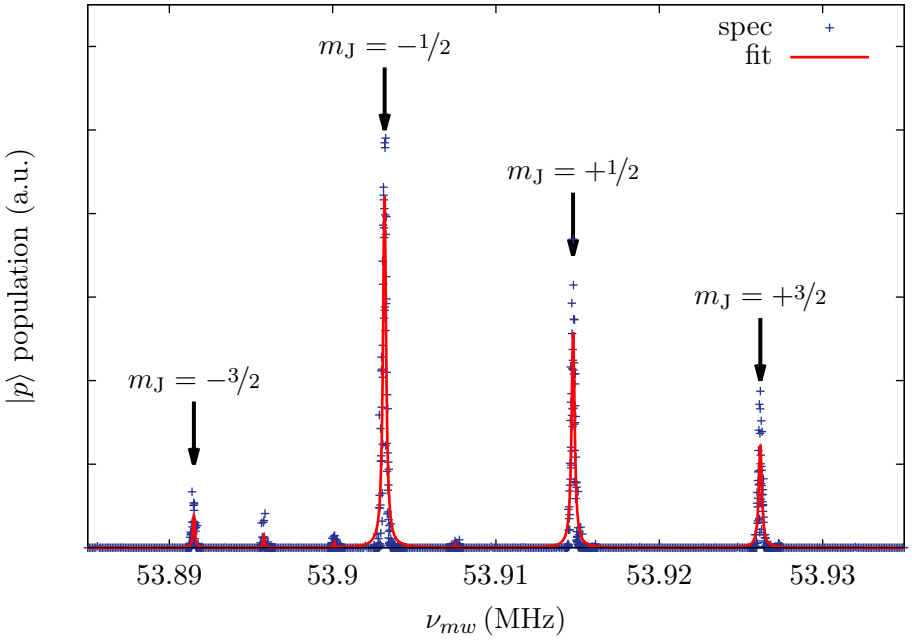

Figure 3.15: Spectroscopy of the microwave coupling: the four marked peaks correspond to the four fine-states in the $|p\rangle$ state manifold. The red line is a Lorentzian fit. The other peaks are due to imperfect preparation of the ground state: in the preparation process there are non-vanishing populations in hyperfine states other than the desired ground state $\left|5S_{1/2}, F = 2, m_F = +2\right\rangle$, which then couple to the $|p\rangle$-state manifold through other excitation channels.

3.5 Comparison to experimental data

The AC-Stark shift can be measured by performing spectroscopy measurements on the microwave coupling, as shown in figure 3.15. For each data point a cloud of ^{87}Rb-atoms is cooled, the Rydberg-P-states are excited, as described in section 3.3, and the Rydberg atoms are ionised and detected by the MCP, as shown in figure 1.1; thereby the fraction of Rydberg atoms can be measured. During one spectroscopy scan, the laser intensities, and thereby the Rabi frequencies, are kept fixed. In order to measure the change in AC-Stark shift another spectroscopy scan is done with a different laser intensity on the probe transition, *i.e.* a different probe Rabi frequency Ω_p. By increasing the probe intensity the peaks in the spectroscopy shift to lower microwave frequencies, which corresponds to an upwards energy shift of the ground state.

The possibility to measure the AC-Stark shift by spectroscopy of the microwave transition opens up a new way of indirectly measuring the probe Rabi frequency: from rewriting equation (2.23) one obtains:

$$\Omega_p = \sqrt{S_g \left(\Delta_e - \frac{|\Omega_c|^2}{\Delta_s} \right)} \tag{3.19}$$

where S_g can be obtained from spectroscopy, and Δ_e and Δ_s are well-known parameters of the laser system. The EIT-splitting of the absorption profile, as shown in figure 1.8 depends on the coupling Rabi frequency Ω_c [14]; thereby, Ω_c can indirectly be measured. The advantage of using the microwave field to measure the strength of the probe field lies in its high accuracy: the spectroscopy can be carried out in steps of the order of 10 kHz which allows for a high precision measurement of Ω_p.

Chapter 4

Summary and Outlook

4.1 Summary

In this thesis it could be shown that the three-photon excitation dynamics in the regime of large intermediate detunings can be understood in terms of a simplified two-level picture, where only two effective parameters are needed to characterise the behaviour. In order to resonantly couple the ground- and the Rydberg-P-state with a three-photon scheme not only the energy difference of the bare atomic states but also the light-induced AC-Stark shifts have to be taken into account. Therefore, to tune the excitation scheme on effective resonance either the AC-Stark shifts can be balanced out, or the three-photon detuning can counteract the difference in AC-Stark shifts.

The effect of the rapidly decaying excited state on the population transfer is small in the parameter regime used in the experiment and can be neglected for most purposes. However, it was shown that this intermediate decay can, in principle, be used to enhance population transfer to the P-state. An effective two-level master equation as well as a simplified dressed-state interpretation of this process were given.

Furthermore, numerical simulations of the full four-level system were carried out. The simulations were used to check the validity of the analytical two-level descriptions: they show good agreement for parameters where the assumption of large intermediate detunings holds. The excitation with finite coupling durations, as used in the experiment, were simulated, and the influence of the different parameters on the population transfer were analysed. With the experimentally highest achievable Rabi frequencies, the possible population transfer was estimated to be over 90%.

By these analytical and numerical results a better understanding of the three-photon excitation was gained, allowing for a simplified optimisation of the laser system to effectively excite Rydberg-P-states in ultracold gases.

4.2 Outlook: measurement of single impurities

As a next step for exploring the dynamics in strongly interacting quantum systems, a system for detecting single Rydberg-P-state excitations is developed. In this section a short outlook on this project is given.

In a simplified picture, the effect of the long-range Rydberg interactions can be incorporated into an energy shift of the Rydberg levels [9]. In the EIT coupling, the intermediate state is coupled to a Rydberg state which can strongly interact with neighbouring atoms that also have an admixture a Rydberg state—it may be the same or a Rydberg state which is energetically close. Therefore, interactions influence the behaviour of the atom with respect to optical couplings on transitions involving these interacting states. This effect becomes apparent when exciting Rydberg states in a dense ensemble of cold atoms: after one atom is excited, the atoms in its proximity experience an energy shift by which they are effectively tuned out of resonance with respect to the applied excitation scheme, and consequently, these atoms cannot be excited. This effect is called *Rydberg blockade*, and the lengthscale associated with it is expressed through the, so called, *blockade radius* R_b; it is typically of the order of a few µm [9].

Atoms in the ground state can usually be detected using the absorption imaging technique when a suitable closed cycled transition scheme is available. Being excited states with multiple decay channels, Rydberg atoms do not fulfil this requirement, and another method is needed to optically detect them. Few approaches have been proposed and developed [39, 40]. The one that is used in this experiment, called *Interaction-Enhanced Imaging* (IEI), leverages three effects: the Rydberg blockade to have Rydberg atoms spatially separated more than the imaging system's optical resolution, electromagnetically induced transparency (EIT) to translate optical properties of the Rydberg state onto the imaging transition and the strong Rydberg-Rydberg interactions to locally change the susceptibility of the atom cloud around the Rydberg atom that is to detect.

In this chapter the following set-up—also shown in figure 4.1—is considered: a cloud of, so called *probe atoms*, which are ground-state atoms with a small admixture of an $|ns\rangle$ state from the EIT-coupling, with a small number of highly excited Rydberg atoms, the so called *impurities*, in state $|n'p\rangle$. The impurities can be imagined to be in a bath of probe atoms, as $N_{\text{ground state}} \gg N_{\text{impurity}}$.

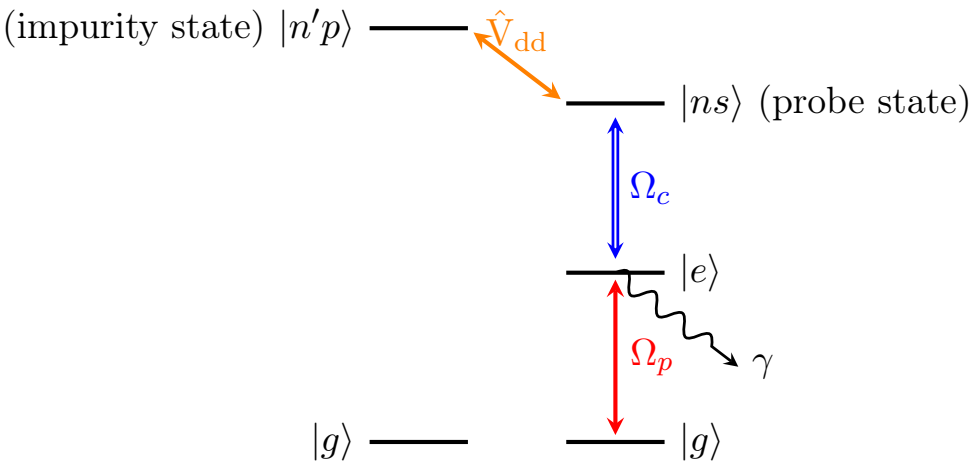

Figure 4.1: Interaction between impurity- and probe-atoms: the impurity atoms (left) in state $|np\rangle$ are coupled to the probe atoms (right) by dipole-dipole interaction.

The basic idea behind the IEI scheme is to use the fact that the presence of the impurity affects the absorption properties of the surrounding probe atoms that, due to EIT coupling, are in a mixed state between the ground- and the Rydberg-state $|ns\rangle$. The interaction induces an energy shift on the $|ns\rangle$ state of the probe atoms, which depends on the distance between the probe- and the impurity-atom. By this interaction induced shift, the coupling-transition $|e\rangle \leftrightarrow |ns\rangle$ is tuned out of resonance with respect to the coupling frequency ν_c. This effectively weakens the the transparency induced by the coupling laser. Hence, in a cloud of ultracold atoms under EIT conditions, the probe atoms in the proximity of an impurity are not transparent for the probe-light and therefore cast a shadow on absorption images of the cloud. This is schematically depicted in figure 4.2. The probe atoms inside the blockade sphere can be imagined to behave as

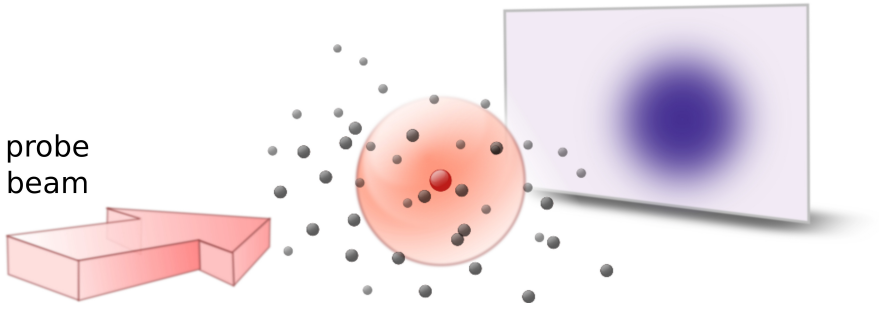

Figure 4.2: EIT-imaging scheme: the probe beam is attenuated by ground-state atoms in the proximity of a Rydberg excitation due to interaction induced level shifts.

two-level absorbers, as depicted in figure 1.7a; whereas the background atoms outside the blockade sphere are under three-level EIT conditions (figure 1.7b). The lengthscale of the EIT-weakening caused by interaction is given by the blockade radius.

However, so far IEI is limited by the fact that the sensitivity of this method allowed to detect the susceptibility change induced by fewer than ten Rydberg atoms; while they could not be distinguished individually. In order to observe many-body quantum dynamics in more detail, it is desirable to have an imaging method and an optical system that are capable of spatially resolving single Rydberg atoms in a cloud of otherwise unexcited ground-state atoms.

IEI can, in principle, be used to resolve singe impurities. However, there are a few challenges to be met:

1. The impurity excitations can move to one of the neighbouring ground-state atoms; thereby the image is blurred and single impurities may not be resolved.
2. The signal-to-noise ratio (SNR): there are many intrinsic noise sources of the imaging system such as photon shot noise, and detector electronics noise.
3. The signal coming from the atom cloud can be reduced by imperfect EIT conditions due to interactions other than the impurity-probe interactions.

The first problem can be addressed by reducing the cloud to the size of a single blockade sphere. In such a reduced cloud the impurity cannot travel further than the blockade radius, and thus no additional blurring is induced by the Rydberg excitation moving from one atom to another. Obviously, this constraint destroys all possible dynamics between multiple impurities; therefore, this can only be a provisional solution in order to show that single impurity detection is possible in principle.

The intrinsic noise of the imaging system can be overcome by increasing the exposure time for a single image; however, this is limited by the lifetime of the impurity atoms.

The maximum contrast in the absorption image between areas blockaded by an impurity and the surrounding background gas under EIT conditions is given by the difference between the resonant absorption of two-level- and EIT-absorbers (see figure 1.8). In order to have the optimum achievable contrast one needs to have perfect EIT in the background gas, *i.e.* no absorption on resonance. Any distortion of the EIT system, leads to an increase of resonant absorption, which is precisely the effect exploited in the imaging method. However, distortions of the EIT originating from other effects than probe-impurity interactions weaken the signal produced by the cloud. So in order to optimise the signal coming from the cloud one needs to understand how the interactions between probe- and impurity-atoms, and between probe- and other probe-atoms influence the light propagation through cloud under EIT conditions.

In principle it is possible to formulate such a problem in the full density matrix description. However, the dipole-dipole operator (1.5) couples the atoms, such that they can no longer be described in terms of single-atom density matrices. In order to consider correlations between all atoms in an N-atom system, the density operator needs to be expressed in terms of N-particle product states:

$$|\psi\rangle = |\psi_1\rangle \otimes |\psi_2\rangle \otimes \cdots \otimes |\psi_N\rangle \,. \tag{4.1}$$

Let the problem be reducible to η states for each atom; then the number of entries in the density matrix scales as η^{2N}, and therefore increases exponentially with the atom number. In general, problems involving such large density matrices are neither analytically solvable nor can they be tackled numerically for atom numbers comparable to typical experiments. At best, numerical solutions of EIT with interactions using the full density matrix are limited to a handful of atoms. To overcome these computational difficulties the system needs to be simplified, *e.g.* by including interactions as mere level shifts and neglecting interatomic correlations. How EIT is influenced by interparticle interactions is still not fully understood and an open question for current research. Many theoretical [41–48] as well as experimental [8] investigations have been carried out in this field.

Being able to resolve single impurities in ultracold Rydberg gases will enable full access to the dynamics of such a system. This would open the possibility to address fundamental questions about coherent-quantum and open-system dynamics in a variety of settings, exploiting the enhanced interaction properties of Rydberg atoms.

Bibliography

[1] V. I. Balykin, V. G. Minogin, and V. S. Letokhov. Electromagnetic trapping of cold atoms. *Reports on Progress in Physics*, 63(9):1429, 2000. URL http://stacks.iop.org/0034-4885/63/i=9/a=202.

[2] R. Grimm, M. Weidemüller, and Y. B. Ovchinnikov. Optical Dipole Traps for Neutral Atoms. *Advances in Atomic Molecular and Optical Physics*, 42:95–170, 2000. doi: 10.1016/S1049-250X(08)60186-X.

[3] M. Greiner, O. Mandel, T. Esslinger, T. W. Hansch, and I. Bloch. Quantum phase transition from a superfluid to a mott insulator in a gas of ultracold atoms. *Nature*, 415(6867):39–44, 01 2002. URL http://dx.doi.org/10.1038/415039a.

[4] M. Saffman, T. G. Walker, and K. Mølmer. Quantum information with rydberg atoms. *Rev. Mod. Phys.*, 82:2313–2363, Aug 2010. doi: 10.1103/RevModPhys.82.2313. URL http://link.aps.org/doi/10.1103/RevModPhys.82.2313.

[5] M. D. Lukin, M. Fleischhauer, R. Cote, L. M. Duan, D. Jaksch, J. I. Cirac, and P. Zoller. Dipole blockade and quantum information processing in mesoscopic atomic ensembles. *Phys. Rev. Lett.*, 87:037901, Jun 2001. doi: 10.1103/PhysRevLett.87.037901. URL http://link.aps.org/doi/10.1103/PhysRevLett.87.037901.

[6] G. Günter, H. Schempp, M. Robert-de Saint-Vincent, V. Gavryusev, S. Helmrich, C. S. Hofmann, S. Whitlock, and M. Weidemüller. Observing the dynamics of dipole-mediated energy transport by interaction-enhanced imaging. *Science*, 342(6161):954–956, 11 2013. doi: 10.1126/science.1244843. URL http://www.sciencemag.org/content/342/6161/954.abstract.

[7] A. Gaj, A. T. Krupp, J. B. Balewski, R. Löw, S. Hofferberth, and T. Pfau. From molecular spectra to a density shift in dense Rydberg gases. *Nature Communications*, 5:4546, August 2014. doi: 10.1038/ncomms5546.

[8] J. Pritchard. *Cooperative Optical Non-linearity in a blockaded Rydberg Ensemble*. PhD thesis, Durham University, 2011.

[9] R. Löw, H. Weimer, J. Nipper, J. B. Balewski, B. Butscher, H. P. Büchler, and T. Pfau. An experimental and theoretical guide to strongly interacting rydberg gases. *Journal of Physics B: Atomic, Molecular and Optical Physics*, 45(11):113001, 2012. URL http://stacks.iop.org/0953-4075/45/i=11/a=113001.

[10] T. Pohl, C. S. Adams, and H. R. Sadephpour. Cold rydberg gases and ultra-cold plasmas. *Journal of Physics B: Atomic, Molecular and Optical Physics*, 44(18): 180201, 2011. URL http://stacks.iop.org/0953-4075/44/i=18/a=180201.

[11] N. Bohr. On the constitution of atoms and molecules. *Philosophical Magazine Series 6*, 26(151):1–25, 1913. doi: 10.1080/14786441308634955. URL http://dx.doi.org/10.1080/14786441308634955.

[12] T. F. Gallagher. *Rydberg atoms*. Number 3 in Cambridge monographs on atomic, molecular, and chemical physics. Cambridge Univ. Press, Cambridge, digitally print. 1. pbk version edition, 2005. ISBN 0-521-02166-9 ; 978-0-521-02166-1.

[13] T. F. Gallagher. Rydberg atoms. *Reports on Progress in Physics*, 51(2):143, 1988. URL http://stacks.iop.org/0034-4885/51/i=2/a=001.

[14] G. Günter. *Interfacing Rydberg atoms with light and observing their interaction driven dynamics*. PhD thesis, Heidelberg, Univ., Diss., 2014, 2014. Mit e. Zsfass. in dt. u. engl. Sprache.

[15] C. S. Hofmann, G. Günter, H. Schempp, N. L. M. Müller, A. Faber, H. Busche, M. Robert-de Saint-Vincent, S. Whitlock, and M. Weidemüller. An experimental approach for investigating many-body phenomena in rydberg-interacting quantum systems. *Frontiers of Physics*, 9(5):571–586, 2014. ISSN 2095-0462. doi: 10.1007/s11467-013-0396-7. URL http://dx.doi.org/10.1007/s11467-013-0396-7.

[16] D. A. Steck. *Quantum and Atom Optics*. available online at http://steck.us/teaching (revision 0.10.0, 3 September 2014).

[17] M. O. Scully and M. S. Zubairy. *Quantum optics*. Cambridge Univ. Press, Cambridge [u.a.], 6. print. edition, 2008. ISBN 978-0-521-43595-6 ; 0-521-43595-1 ; 0-521-43458-0 ; 978-0-521-43458-4.

[18] C. Cohen-Tannoudji, J. Dupont-Roc, and G. Grynberg. *Atom-photon interactions*. Physics textbook. Wiley-VCH, Weinheim, 2004. ISBN 0-471-29336-9 ; 978-0-471-29336-1.

[19] P. Lambropoulos and D. Petrosyan. *Fundamentals of quantum optics and quantum information*. Springer, Berlin ; Heidelberg [u.a.], 2007. ISBN 3-540-34571-X ; 978-3-540-34571-8.

[20] M. Lukin. Lecture notes on modern atomic and optical physics ii. Harvard University.

[21] K. Blum. *Density matrix theory and applications*. Number 64 in Springer series on atomic, optical, and plasma physics ; 64 ; Springer series on atomic, optical, and plasma physics. Springer, Heidelberg [u.a.], 3. ed. edition, 2012. ISBN 978-3-642-20560-6 ; 978-3-642-20561-3. 1. Aufl. 1981. - 2. Aufl. 1996.

[22] R. R. Puri. *Mathematical methods of quantum optics*. Number 79 in Springer series in optical sciences ; 79 ; Physics and astronomy online library ; Springer series in optical sciences. Springer, Berlin ; Heidelberg [u.a.], 2001. ISBN 3-540-67802-6 ; 978-3-540-67802-1.

[23] G. Lindblad. On the generators of quantum dynamical semigroups. *Communications in Mathematical Physics*, 48(2):119–130, 1976. ISSN 0010-3616. doi: 10.1007/BF01608499. URL http://dx.doi.org/10.1007/BF01608499.

[24] B. W. Shore and P. L. Knight. The jaynes-cummings model. *Journal of Modern Optics*, 40(7):1195–1238, 1993. doi: 10.1080/09500349314551321. URL http://dx.doi.org/10.1080/09500349314551321.

[25] H. Carmichael. *Master equations and Fokker-Planck equations*. Texts and monographs in physics. Springer, Berlin ; Heidelberg [u.a.], 1999. ISBN 3-540-54882-3 ; 978-3-540-54882-9.

[26] S. Sultana and M. S. Zubairy. Effect of finite bandwidth on refractive-index enhancement and lasing without inversion. *Phys. Rev. A*, 49:438–448, Jan 1994. doi: 10.1103/PhysRevA.49.438. URL http://link.aps.org/doi/10.1103/PhysRevA.49.438.

[27] J. Otterbach. *Single- and Many-body Phenomena of Dark-state Polaritons*. PhD thesis, TU Kaiserslautern, 2011. URL https://books.google.de/books?id=lTVcMwEACAAJ.

[28] M. Fleischhauer, A. Imamoglu, and J. P. Marangos. Electromagnetically induced transparency: Optics in coherent media. *Rev. Mod. Phys.*, 77:633–673, Jul 2005. doi: 10.1103/RevModPhys.77.633. URL http://link.aps.org/doi/10.1103/RevModPhys.77.633.

[29] C. Ates. *Anregungsdynamik ultrakalter Rydberggase*. PhD thesis, TU Dresden, 2009.

[30] C. Ates, T. Pohl, T. Pattard, and J. M. Rost. Antiblockade in rydberg excitation of an ultracold lattice gas. *Phys. Rev. Lett.*, 98:023002, Jan 2007. doi: 10.1103/

PhysRevLett.98.023002. URL http://link.aps.org/doi/10.1103/PhysRevLett.98.023002.

[31] B. Huber, T. Baluktsian, M. Schlagmüller, A. Kölle, H. Kübler, R. Löw, and T. Pfau. Ghz rabi flopping to rydberg states in hot atomic vapor cells. *Phys. Rev. Lett.*, 107: 243001, Dec 2011. doi: 10.1103/PhysRevLett.107.243001. URL http://link.aps.org/doi/10.1103/PhysRevLett.107.243001.

[32] F. Reiter and A. S. Sørensen. Effective operator formalism for open quantum systems. *Phys. Rev. A*, 85:032111, Mar 2012. doi: 10.1103/PhysRevA.85.032111. URL http://link.aps.org/doi/10.1103/PhysRevA.85.032111.

[33] C. Goren, A. D. Wilson-Gordon, M. Rosenbluh, and H. Friedmann. Atomic four-level n systems. *Phys. Rev. A*, 69:053818, May 2004. doi: 10.1103/PhysRevA.69.053818. URL http://link.aps.org/doi/10.1103/PhysRevA.69.053818.

[34] K. Bergmann, H. Theuer, and B. W. Shore. Coherent population transfer among quantum states of atoms and molecules. *Rev. Mod. Phys.*, 70:1003–1025, Jul 1998. doi: 10.1103/RevModPhys.70.1003. URL http://link.aps.org/doi/10.1103/RevModPhys.70.1003.

[35] V. S. Malinovsky and D. J. Tannor. Simple and robust extension of the stimulated raman adiabatic passage technique to n-level systems. *Phys. Rev. A*, 56:4929–4937, Dec 1997. doi: 10.1103/PhysRevA.56.4929. URL http://link.aps.org/doi/10.1103/PhysRevA.56.4929.

[36] J. Deiglmayr, M. Reetz-Lamour, T. Amthor, S. Westermann, A.L. de Oliveira, and M. Weidemüller. Coherent excitation of rydberg atoms in an ultracold gas. *Optics Communications*, 264(2):293 – 298, 2006. ISSN 0030-4018. doi: http://dx.doi.org/10.1016/j.optcom.2006.02.058. URL http://www.sciencedirect.com/science/article/pii/S0030401806004901. Quantum Control of Light and Matter In honor of the 70th birthday of Bruce Shore.

[37] B. Zhang, J.-H. Wu, X.-Z. Yan, L. Wang, X.-J. Zhang, and J.-Y. Gao. Coherence generation and population transfer by stimulated raman adiabatic passage and π pulse in a four-level ladder system. *Opt. Express*, 19(13):12000–12007, Jun 2011. doi: 10.1364/OE.19.012000. URL http://www.opticsexpress.org/abstract.cfm?URI=oe-19-13-12000.

[38] H. Kreiss and O. E. Ortiz. *Introduction to numerical methods for time dependent differential equations*. J. Wiley & Sons, Hoboken, NJ, online-ausg. edition, 2014. ISBN 1-118-83891-2 ; 978-111-883-891-4 ; 978-111-883-895-2 ; 978-1-118-83891-4. URL http://proquest.tech.safaribooksonline.de/9781118838914.

[39] G. Günter, M. Robert-de Saint-Vincent, H. Schempp, C. S. Hofmann, S. Whitlock, and M. Weidemüller. Interaction enhanced imaging of individual rydberg atoms in dense gases. *Phys. Rev. Lett.*, 108:013002, Jan 2012. doi: 10.1103/PhysRevLett.108.013002. URL http://link.aps.org/doi/10.1103/PhysRevLett.108.013002.

[40] B. Olmos, W. Li, S. Hofferberth, and I. Lesanovsky. Amplifying single impurities immersed in a gas of ultracold atoms. *Phys. Rev. A*, 84:041607, Oct 2011. doi: 10.1103/PhysRevA.84.041607. URL http://link.aps.org/doi/10.1103/PhysRevA.84.041607.

[41] J. Stanojevic, V. Parigi, E. Bimbard, A. Ourjoumtsev, and P. Grangier. Dispersive optical nonlinearities in a rydberg electromagnetically-induced-transparency medium. *Phys. Rev. A*, 88:053845, Nov 2013. doi: 10.1103/PhysRevA.88.053845. URL http://link.aps.org/doi/10.1103/PhysRevA.88.053845.

[42] C. Ates, S. Sevinçli, and T. Pohl. Electromagnetically induced transparency in strongly interacting rydberg gases. *Phys. Rev. A*, 83:041802, Apr 2011. doi: 10.1103/PhysRevA.83.041802. URL http://link.aps.org/doi/10.1103/PhysRevA.83.041802.

[43] D. Petrosyan, J. Otterbach, and M. Fleischhauer. Electromagnetically induced transparency with rydberg atoms. *Phys. Rev. Lett.*, 107:213601, Nov 2011. doi: 10.1103/PhysRevLett.107.213601. URL http://link.aps.org/doi/10.1103/PhysRevLett.107.213601.

[44] K. P. Heeg, M. Gärttner, and J. Evers. Hybrid model for rydberg gases including exact two-body correlations. *Phys. Rev. A*, 86:063421, Dec 2012. doi: 10.1103/PhysRevA.86.063421. URL http://link.aps.org/doi/10.1103/PhysRevA.86.063421.

[45] J. Reslen. Many-body effects in a model of electromagnetically induced transparency. *Journal of Physics B: Atomic, Molecular and Optical Physics*, 44(19): 195505, 2011. URL http://stacks.iop.org/0953-4075/44/i=19/a=195505.

[46] M. Gärttner, S. Whitlock, D. W. Schönleber, and J. Evers. Semianalytical model for nonlinear absorption in strongly interacting rydberg gases. *Phys. Rev. A*, 89:063407, Jun 2014. doi: 10.1103/PhysRevA.89.063407. URL http://link.aps.org/doi/10.1103/PhysRevA.89.063407.

[47] M. Gärttner and J. Evers. Nonlinear absorption and density-dependent dephasing in rydberg electromagnetically-induced-transparency media. *Phys. Rev. A*, 88:033417, Sep 2013. doi: 10.1103/PhysRevA.88.033417. URL http://link.aps.org/doi/10.1103/PhysRevA.88.033417.

[48] S. Sevinçli, N. Henkel, C. Ates, and T. Pohl. Nonlocal nonlinear optics in cold rydberg gases. *Phys. Rev. Lett.*, 107:153001, Oct 2011. doi: 10.1103/PhysRevLett.107.153001. URL http://link.aps.org/doi/10.1103/PhysRevLett.107.153001.

Erklärung

Ich versichere, dass ich diese Arbeit selbstständig verfasst und keine anderen als die angegebenen Quellen und Hilfsmittel benutzt habe.

Heidelberg, den 28.8.2015,